Journal of Metals, Materials and Minerals, 34(3), 2084, 2024

A review on the development of metals-doped Vanadium oxides for zinc-ion battery

Kittima LOLUPIMAN[1,2], Jin CAO[3,*], Dongdong ZHANG[4], Chengwu YANG[2], Xinyu ZHANG[5], and Jiaqian QIN[2,*]

[1] *The Nanoscience and Technology program, Graduate School, Chulalongkorn University, Soi Chula 12, Phayathai Road, Wangmai, Pathumwan, Bangkok 10330, Thailand*
[2] *Center of Excellence on Advanced Materials for Energy Storage, Metallurgy and Materials Science Research Institute (MMRI), Chulalongkorn University, Soi Chula 12, Phayathai Road, Wangmai, Pathumwan, Bangkok 10330, Thailand*
[3] *College of Hydraulic & Environmental Engineering, China Three Gorges University, Yichang, Hubei 443002, China*
[4] *School of Materials Science and Engineering, Shenyang University of Technology, Shenyang 110870, China*
[5] *State Key Laboratory of Metastable Materials Science and Technology, Yanshan University, Qinhuangdao, 066004 P. R. China*

***Corresponding author e-mail**: jiaqian.q@chula.ac.th, caojin@ctgu.edu.cn

Received date:
12 June 2024
Revised date:
28 July 2024
Accepted date:
20 August 2024

Keywords:
Aqueous zinc ion batteries;
Cathode materials;
Vanadium-base compounds;
Vanadium oxides

Abstract

Rechargeable zinc-ion batteries (ZIBs) are emerging as promising energy storage devices for various applications, including large-scale energy storage, due to their environmental friendliness, enhanced safety, and low cost. A key challenge in ZIB development is creating cathode materials that reduce the solubility of active materials in aqueous electrolytes, increase electrical conductivity, and extend life cycles for high performance. Vanadium-based compounds, with their diverse structures and multiple oxidation states (+2, +3, +4, and +5), have been extensively studied as effective cathodes for ZIBs. This mini review highlights recent research on doping transition metals into vanadium oxide materials to achieve superior electrochemical performance compared to electrodes prepared via solid-phase synthesis and hydrothermal methods. Additionally, it offers guidance for the future development of vanadium-based materials.

1. Introduction

1.1 Batteries

Batteries are devices that store and release electrical energy through chemical reactions that store energy generated from renewable sources including solar energy, geothermal energy, bioenergy, hydropower, tidal and ocean energy [1] for later use or in emergency backup systems become the most widely used energy storage technology. Especially, electrical energy storage systems (EESS) some types of batteries as shown in Figure 1 [2] must have large-scale batteries used to store spare energy generated by power plants during periods of low demand. This spare energy can be released during peak demand times, helping to stabilize the electrical grid.

Battery energy storage (BES) has 2 common types of batteries, Type 1: primary or non-rechargeable batteries are designed for one-time use and cannot be reused because the electrochemical reaction cannot be reversible. Examples are zinc-carbon batteries (Leclanche batteries), metal-air batteries (Al, Fe, Mg, Cd and Zn), manganese-alkaline batteries, lithium-manganese dioxide batteries (Li-MnO_2), lithium iron disulfide (Li-FeS_2) [3-5]. These are widely used in many applications due to their high energy density, long lifespan and cost-effectiveness. Alkaline batteries are the standard choice for most remote controls, small handheld calculators and analog and digital clocks often use them. Especially those requiring high power output like toys, flashlights, sensors and monitoring devices also use alkaline batteries for long-term deployments) [3]. Batteries with long shelf life, like lithium, are preferred for devices that may be stored for extended periods. In summary, while primary batteries have their place in certain applications, their limitations in terms of sustainability, cost-effectiveness, and performance. Type 2: secondary or rechargeable batteries can be recharged multiple times. Examples, Lead-acid batteries are widely used for automotive (starting, lighting), UPS systems, and stationary energy storage owing to their low cost and high current output on the other hand the big size with heavy weight affects low energy density and poor cycle life compared to other types. Nickel-cadmium (Ni-Cd) batteries are used for power tools with good performance at low temperatures and long cycle life but environmental concerns due to cadmium. Nickel-metal hydride (NiMH) batteries have a higher energy density than NiCd but still lower energy density than lithium-ion and are used for hybrid electric vehicles. Lithium-ion (Li-ion) batteries have become the most popular battery in recent years. Their high energy density, long cycle life, and relatively high power output have made them the preferred choice for various applications such as smartphones, laptops, electric vehicles and energy storage [3,4,6,7]. However, these batteries still have some limitations and

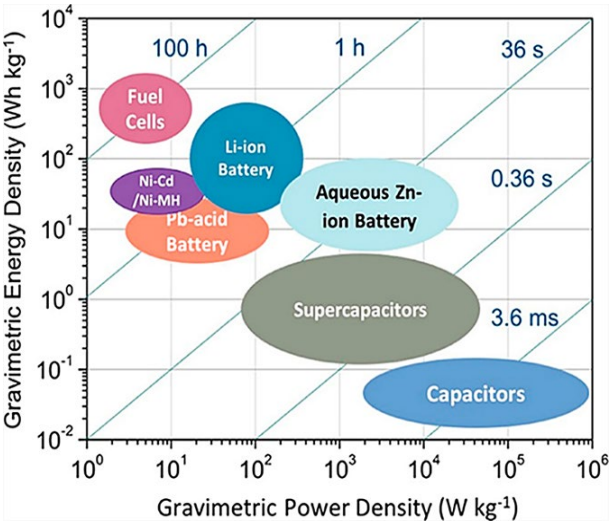

Figure 1. Ragone plot of several electrical energy storage systems (EESS) [2].

Figure 2. Overview of zinc-ion batteries [36].

we will discuss this in more detail in the next subsection. Two types of battery systems are different in their ability to be reused. The desired operating time of the device determines the battery type and size. Each type has its own set of characteristics, advantages, and disadvantages, making them suitable for different applications. This article review provides a comprehensive summary of the recent cathode materials. Especially, the development of vanadium-based cathode material via metal doping elements will be discussed in the next section.

1.2 Lithium-Ion Batteries (LIBS)

Lithium-ion batteries (LIBS) are among the most popular and widely used in various applications. They are commonly operating in small electronic devices, electric vehicles (EV), electrical renewable energy storage systems, and many other technologies due to their high operating voltage (~ 3.7 V) with high energy and power density, low self-discharge reaction, operating in various range of temperature and lightweight design [4,6].

However, they also have limitations, such as safety concerns especially if damaged or improperly charged, which can cause thermal runaways and fires due to lithium-ion batteries using flammable organic electrolytes, and the lithium resource available is not being distributed globally can affect the supply chain and high price [7-9].

1.3 Aqueous Zinc Ion Batteries (AZIBS)

At present several alternative battery technologies to solve the limitations associated with traditional lithium-ion batteries. One interesting alternative battery technology is the aqueous zinc ion batteries (AZIBS) [10,11] are rechargeable battery that uses Zn^{2+} as charge carriers with high performance and can be operated with an aqueous electrolyte, which means the electrolyte is composed mainly of water. Aqueous systems have several advantages over non-aqueous systems, such as lower cost, increased safety because of their non-flammability of aqueous solution, and environmental friendliness [2,10,12,13].

The components of aqueous zinc-ion batteries consist of four parts, First, the anode in AZIBs is typically made of metallic zinc (zinc foil, electrodeposition on substrate and zinc nanoparticles) during the discharge process, zinc atoms are oxidized to release zinc ions and electrons [14]. Second, the cathode material can vary, but common materials include manganese-based (MnO_2, Mn_3O_4 [15-17]) vanadium-based (V_2O_5 [18-22], VO_2 [23], $Zn_3(OH)_2V_2O_7{\cdot}2H_2O$, $Zn_2V_2O_7$ [24,25] and V_3O_8) [26,27] or organic and other cathode materials [21,28]. During the discharge process, Zn^{2+} from the anode moves to the cathode and captures electrons. Third, the electrolyte allows ions moving between the anode and cathode in this system using an aqueous solution containing zinc ions. Unlike non-aqueous systems, which use organic solvents, AZIBs use water-based electrolytes [29-32]. This contributes to the safety and cost-effectiveness of the system. Fourth, the separator is like other batteries, AZIBs include a separator that protects direct contact between the anode and cathode to avoid a short circuit while allowing the flow of ions, commonly using a glass fiber separator [33-35].

While aqueous zinc-ion batteries show promise for various applications, they also have several challenges and limitations are including, On the anode, zinc dendrite formation on the surface can pose a safety risk and lead to short circuits within the battery. Dendrites can penetrate the separator and compromise the integrity of the battery, affecting its performance [37,38]. On the cathode side, some cathode materials have high dissolution of elements in the aqueous electrolytes system, which affects poor cycling stability, leading to a gradual degradation of capacity over multiple charge-discharge cycles and may exhibit limited stability or low capacity. Also, the kinetics reaction of aqueous zinc-ion insertion and extraction at the cathode can be slower compared to some other battery systems [39-41]. This can impact the rate capability and efficiency of the aqueous zinc-ion batteries. [52]. Therefore, suitable cathode materials is crucial in enhancing the performance of zinc-ion batteries. Vanadium compounds, which come in various structures and can exist in multiple charged states, are considered good candidates for the cathode material but still have challenges and limitations there are low electrical conductivity in their pure form. Also, the kinetics reaction are slower compared to some other battery systems.

Cathode materials, as the most important parts of zinc-ion batteries. The improvement of cathode materials to reduce the solubility of active material in aqueous electrolytes, increase electrical conductivity and suppress dissolution of active materials and unexpected byproducts in the aqueous solution to improve high performance of zinc-ion batteries including large operating voltage windows, reversible capacity and life cycle stability there are of the challenges.

2. Developing cathode materials

2.1 Manganese-based cathode

Previous research shows results that these batteries use manganese-based as a cathode, Pang, S.C. synthesized MnO_2 nanostructures via hydrothermal and various aging times and temperature by spherical agglomerates formed at lower temperatures and short aging times. At higher temperatures and longer aging, nanorods formed. δ-MnO_2 has phase changes to α-MnO_2 in the range of low to high temperature [42,43].

α-MnO_2 is the common cathode with a symmetric tunnel structure of a [2 × 2] in cross-section. The first research group Xu C. *et al.,* [15] synthesized α-$_{MnO2}$ via the use of hydrothermal following Pang, S. C. [42] and reported a novel zinc-ion battery system with metal Zn as an anode, α-MnO_2 as a cathode (host material), the aqueous electrolyte 2M $ZnSO_4$ and 3M $Zn(NO_3)_2$ were used in this system to compare the performance and then they found that Zn^{2+} ions can be reversibly into the host material which capacity~ 210 mAh·g^{-1}.

Toupin M. *et al.* reported that a MnO_2 powder can be synthesized by mixing $KMnO_4$ and $MnSO_4{\cdot}H_2O$, after that a dark brown residue was obtained. To confirm the morphology by XRD pattern and SEM as shown α-MnO_2 with spherical grains. They reported the electrochemical behavior of MnO_2 powder that has a cyclic voltammogram, CV looks like a previous report with capacity of 150 F·g^{-1} [44].

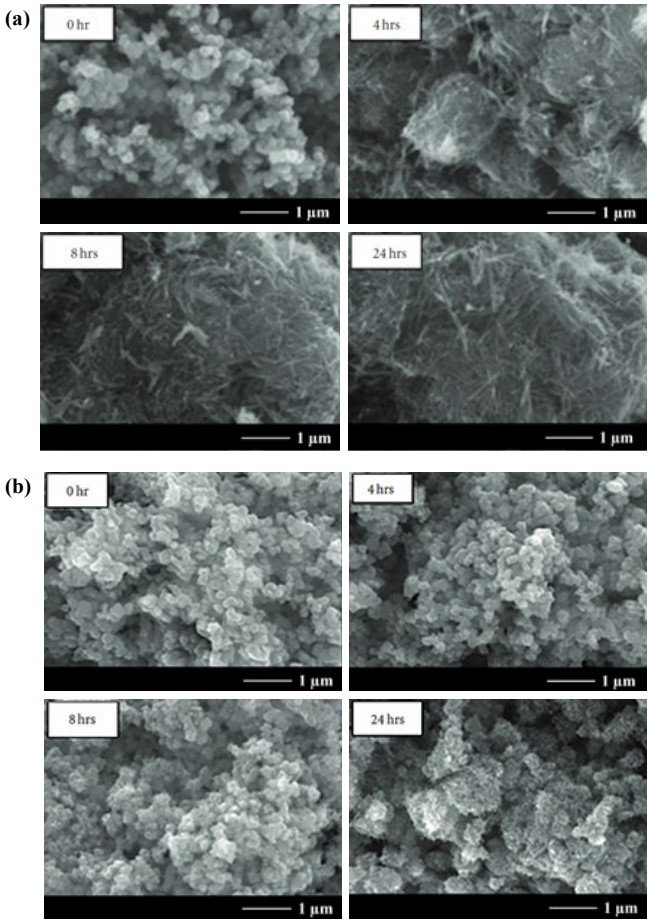

Figure 3. SEM image of MnO_2 various aging time (a) at 25°C and (b) at 80°C [42].

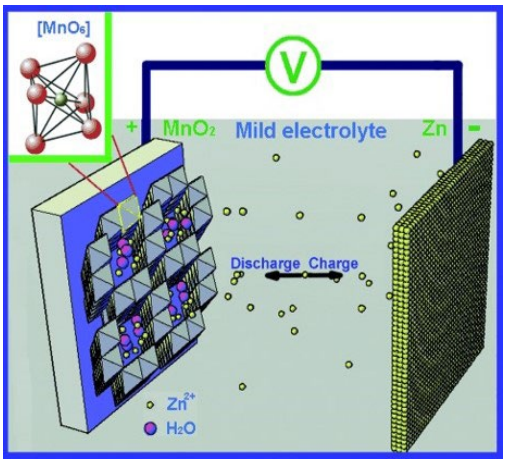

Figure 4. Schematics of the chemical reaction of the zinc ion battery [15].

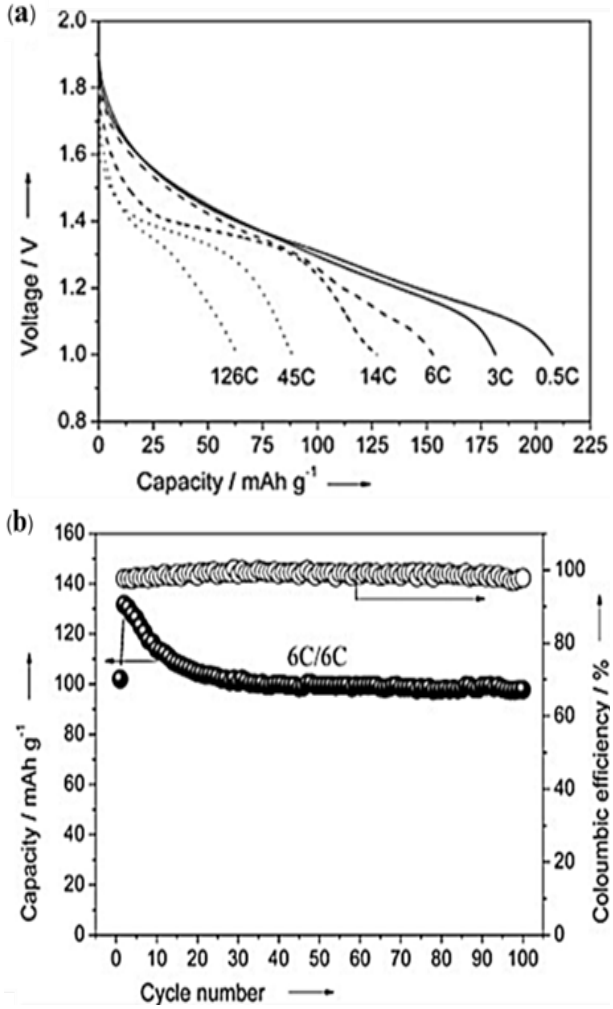

Figure 5. (a) Discharge curves of the ZIB at different current densities and (b) Cycle performance [15].

Islam S. *et al.,* presented β-MnO_2 nanorods can synthesized by microwave-hydrothermal at 200°C, 10 min with the highest stable structure of 1 × 1 tunnel-type, (101) planes which share corners of octahedra MnO_6 in single chains but it has a narrow tunnel affected with low discharge capacity ~270 mAh·g^{-1} at current density 100 mA·g^{-1} and the structure transformed to a spinel structure after long cycles [16].

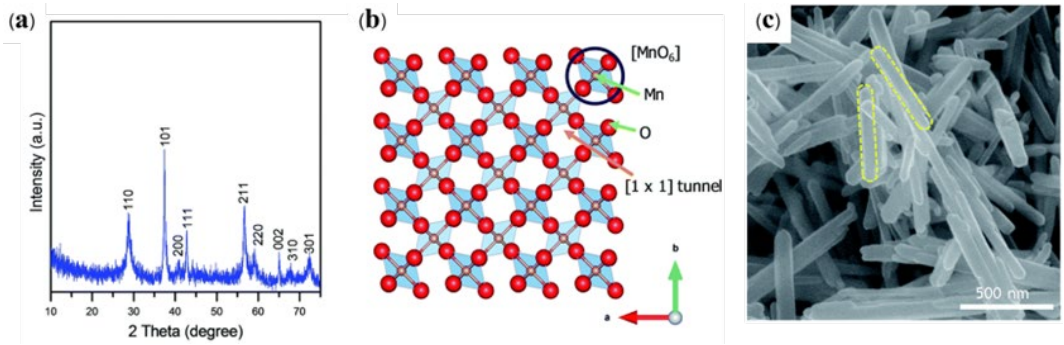

Figure 6. (a) XRD pattern, (b) crystallographic structure and (c) FE-SEM of β-MnO_2 nanorods [16].

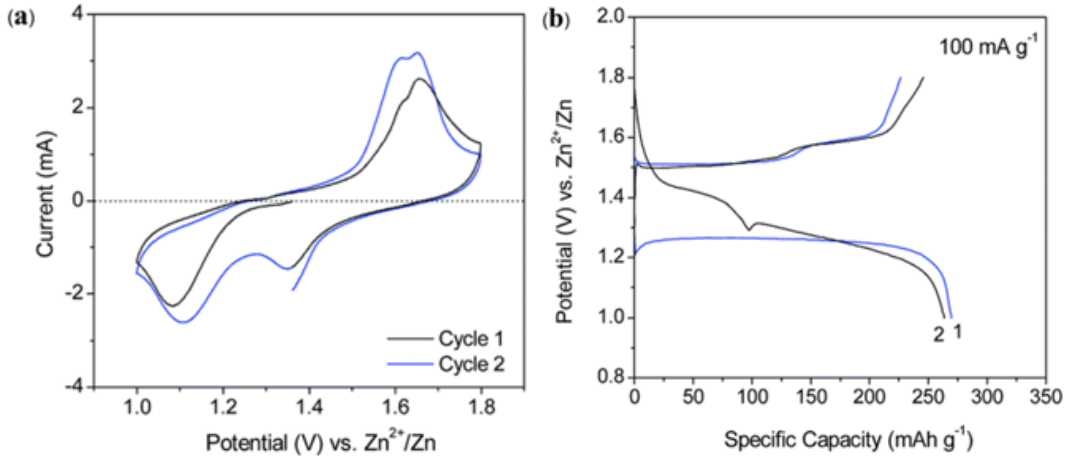

Figure 7. (a) CV profile at scan rate 0.5 $mV \cdot s^{-1}$ and (b) 1st charge and discharge profiles [16].

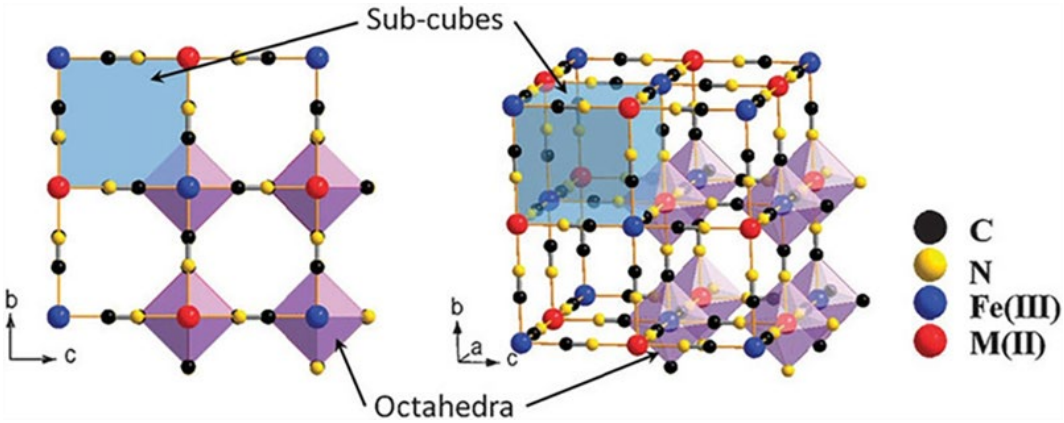

Figure 8. The framework of Prussian blue analogs [45].

Manganese-based materials are excellent cathodes for zinc-ion batteries with high cycle stability due to higher Zn^{2+} insertion and high-capacity retentions. On the other hand, it has a high dissolution of Mn^{2+} into the electrolyte effects on fast capacity decreasing and the slower dynamics reaction are due to the strong reaction between Zn^{2+} and the host materials.

2.2 Prussian Blue Analogs (PBAs)

Prussian blue analogs (PBAs) also known as metal hexacyanometallates by face center cubic structures, FCC have mixed valence with large ionic channels and number of interstitial sites in the lattice can react with the storage sites for some ions, such as Zn^{2+}, Al^{3+}, etc. The common formula of a PBA system can be $A_xMA_y[MB(CN)_6]_z \cdot n\ H_2O$, by A as alkali metal (Li, K, Na) and MA, MB is normally as metal cations (Fe, Co, Cu, Mn or Ni). The synthesis of PBAs can be produced via co-precipitation, electrochemical deposition, etching and ball milling. Both methods are facile and can be developed for large-scale applications.

Liu Z. *et al.*, They mixed $K_3Fe(CN)_6$ and aqueous $FeCl_3$ via a solution precipitation method. Finally, a dark green precipitate that is $FeFe(CN)_6$ nanoparticles was observed. The sample was characterized the morphology by TEM as shown in Figure 9 with a nano cubic shape. The electrochemical performance of the $FeFe(CN)_6$ was studied with the aqueous electrolyte in a zinc ion battery presented the cyclic

voltammetry (CV) with operating voltage in a range of 1.0 V to 2.0 V showing reduction at 1.34 and oxidation at 1.47 V and specific capacity ~120 mAh·g^{-1} at 0.1 C with an open-circuit potential (OCP) ~1.56 V [46].

Xue Y. *et al.* presented a vanadium hexacyanoferrate (VHCF) nanoparticle prepared by $VOSO_4{\cdot}xH_2O$ and $K_3Fe(CN)_6$ is grown on CNT by co-precipitation as shown in the Figure 10 [47]. The micro-structure was analyzed by SEM and TEM, the initial VHCF is an agglomerate of nanoparticles size of 30 nm. The electrochemical obtained the discharge capacity of VHCF/CNTs and VHCF are 97.8 mAh·g^{-1} and 78.5 mAh·g^{-1} at 50 mA·g^{-1} respectively [47].

Prussian blue analogs (PBAs) with mixed valence and many interstitial sites, resulting has efficiency operating at high voltages. However, PBAs still have a lower reversible capacity and poor cycling stability because of severe dissolution and transforming structure after long cycling which is the limitation of this cathode.

Thus, searching for suitable cathode materials is the key point to developing the efficiency of ZIBs with high performance for several applications, especially large-scale electric energy storage. Vanadium-based cathodes with several structures and multi-valent electrons (+2 to +5) are the proper cathode choice for aqueous zinc-ion batteries owing to their excellent Zn^{2+} storage capacity. In this review, the previous research advances of dope elements in vanadium oxide are summarized. The material synthesized strategy and electrochemical performances.

2.3 Vanadium-based cathode

The different valence states of vanadium (+2, +3, +4 and +5) make vanadium-based materials different structures, compositions and electrochemical performance [48]. Thus, vanadium-based materials can contain multiple oxidation states, providing the opportunity for multiple redox reactions during charge and discharge cycles that can contribute to the high reversible capacity and energy density because of multiple valence states and several structures [49]. Vanadium oxides (VO, V_2O_3, VO_2 and V_3O_7 V_2O_5) [50-52], vanadates (non-metal, multivalent metal cations, and monovalent alkali metal cations) [53] all are members of vanadium-based materials.

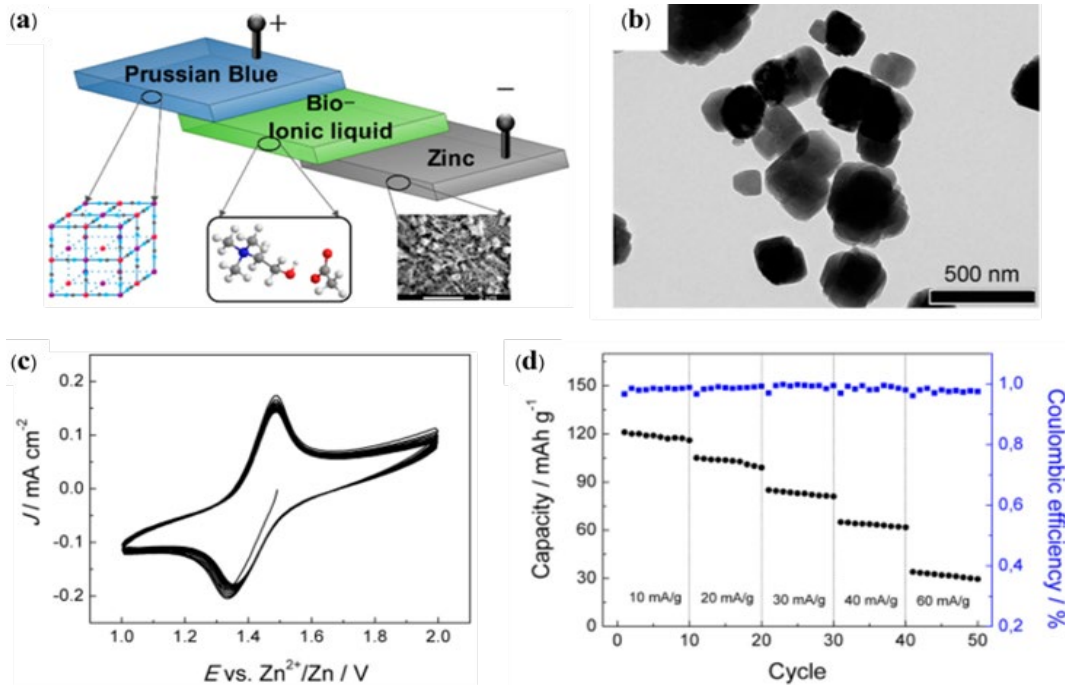

Figure 9. (a) the schematic of Zn//$FeFe(CN)_6$ battery, (b) the TEM image, (c) the CV profile and (d) the rate ability of $FeFe(CN)_6$ at the different current densities [46].

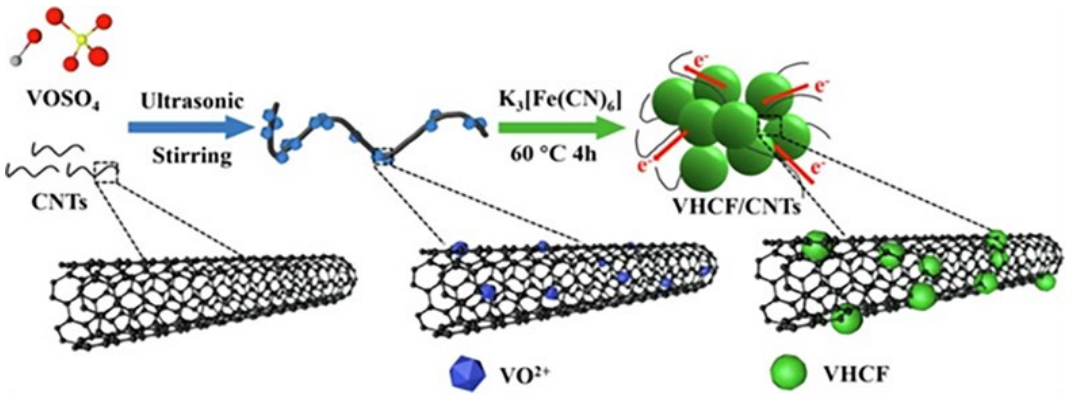

Figure 10. A schematic diagram of the preparation of VHCF/CNTs [47].

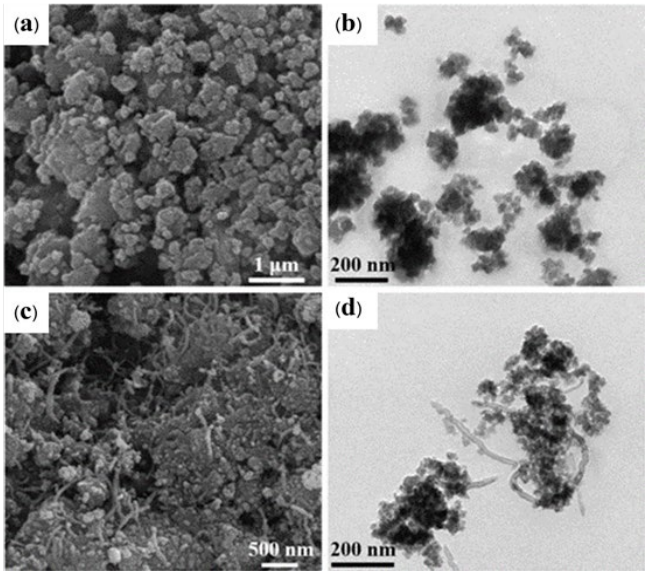

Figure 11. (a,b) SEM-TEM images of VHCF and (c,d) SEM-TEM images of VHCF/CNTs [47].

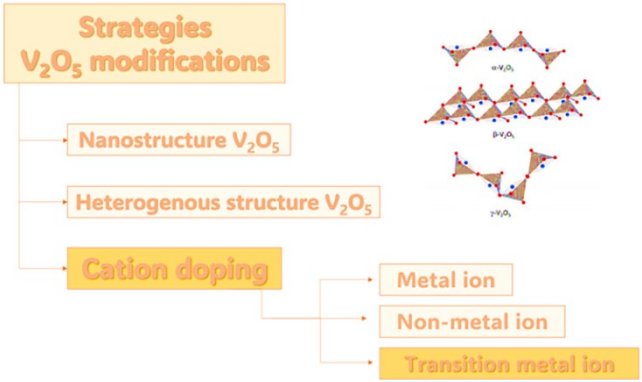

Figure 12. Strategies V_2O_5 modifications [54].

2.3.1 Vanadium pentoxide (V_2O_5)

Vanadium pentoxide (V_2O_5) is considered a promising cathode material for several types of batteries, including lithium-ion batteries (LIBs) and metal-ion batteries (MIBs) as shows high specific capacity and cycling stability. The V_2O_5 often exhibits good reversibility, allowing for efficient cycling during charge and discharge cycles. A reversible cathode is essential for long cycle life and stable battery performance. It is compatible with aqueous electrolytes, making them suitable for use in aqueous battery systems and generally shows good thermal stability, which is crucial for the safety of the battery [52]. Although vanadium oxide cathodes show promise for certain types of batteries but still have specific limitations there are low electrical conductivity in their pure form. Also, the kinetics reaction of insertion and extraction are slower compared to some other battery systems and can result in lower charge/discharge rates due to the V_2O_5 having a small interlayer spacing [54]. The limitation of V_2O_5 can be influenced by various factors and compositions and any doping involves adding small amounts of other elements to modify the properties of the material. This is a modification that can expand interlayered spacing and improve structure stability during the charge and discharge process and expand the cycle stability.

3. Metal-doping Vanadium pentoxide (V_2O_5)

Common transition metals are often used as dopants in V_2O_5 for aqueous zinc-ion batteries. Each metal dopant has unique effects on the electrochemical properties. The metal doping can increase the interlayer spacing and improve the stability of the structure that effected to enhances the electrochemical performance and improves the conductivity of V_2O_5, facilitating faster charge and discharge rates and improving the overall efficiency of the battery. Also, can influence the redox reactions occurring within the cathode and structural stability that leads to improved energy storage capabilities with higher energy density.

Ma L. *et al.* [55] report the synthesis of materials via hydrothermal is a facile method that involves the dissolution of 0.2 M of commercial V_2O_5 and 0.1 M of $Co(CH_3COO)_2 \cdot 4H_2O$ in a 30 mL solution of 1 M acetic acid at a temperature of 200°C for 72 h. Cool down at room temperature and then wash with ethanal Finally, the $Co_{0.247}V_2O_5 \cdot 0.944H_2O$ were received and the morphology were characterized by SEM, TEM and EDS [55] the results in Figure 13.

To investigate the electrochemical performance of the materials, Cyclic voltammetry (CV) profiles of Zn, $Co_{0.247}V_2O_5 \cdot 0.944H_2O$ and $V_2O_5 \cdot nH_2O$ cathode were used to study the reduction reaction by the three electrodes system. This cathode shows reduction reaction peaks as displayed in Figure 14 higher than $V_2O_5 \cdot nH_2O$. The electrochemical impedance spectroscopy (EIS) results insert is corresponding electric circuit diagram. The R_{ct} of this cathode ~16.4 Ω is smaller than the $V_2O_5 \cdot nH_2O$ cathode ~35.3 Ω [55].

To evaluate the battery performance will assembly of a coin cell (CR2032) by Zn as anode $Co_{0.247}V_2O_5 \cdot 0.944H_2O$ as cathode, the result shows cyclic stability and capacity retention ~90.26% after 7500 cycles at 4 $A \cdot g^{-1}$ and assembly of the Zn/Zn symmetrical cell to investigate Zn plating/striping can continuous testing for more than 400 h without ZnO formation on the Zn surface that confirms a dendrite-free on the anode [55]. This cathode material outperforms previous cathode materials of zinc-ion batteries.

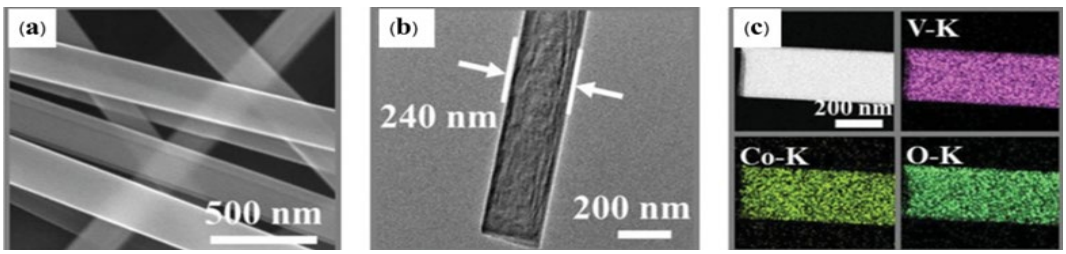

Figure 13. (a) SEM image, (b) TEM image of $Co_{0.247}V_2O_5 \cdot 0.944H_2O$, and (c) EDS mapping [55].

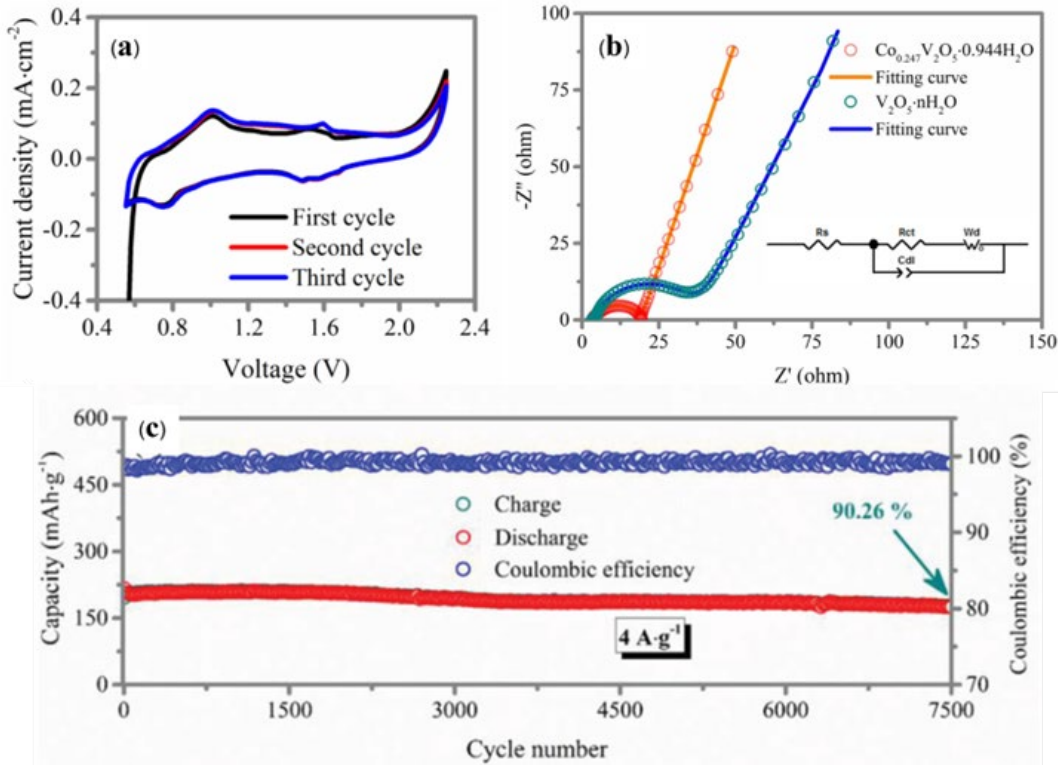

Figure 14. The electrochemical properties (a) cyclic voltammetry profiles, (b) electrochemical impedance spectroscopy, and (c) cycle ability of Zn, $Co_{0.247}V_2O_5{\cdot}0.944H_2O$ and $V_2O_5{\cdot}nH_2O$ [55].

Javed M.S. *et al.* synthesized the 2D V_2O_5-Ti cathode material by V_2O_5 nanosheets were prepared via a facile hydrothermal and then V_2O_5 nanosheets were formed on a Ti-foil via annealing at 300°C in air, 2 h. The morphology and microstructure as shown in Figure 15 [56]. The electrochemical properties of the 2D V_2O_5-Ti cathode was observed, the results at the first discharge and charge process show a high capacity of 503.1 mAh·g^{-1} and 583.0 mAh·g^{-1}, respectively and also have the coulombic efficiency (CE) ~98%.

The 2D V_2O_5-Ti compared with the previous V_2O_5 cathode, this cathode shows a high capacity and CE. They are signifying that the ultra slim nanosheets were grown uniformly which is great conductive Ti-foil can enhance the discharge capacity [56].

Shan L. *et al.* reported that $Ag_{0.4}V_2O_5$ nanobelts was prepared via facile hydrothermal were mixed V_2O_5 with $AgNO_3$ in deionized water at 40°C. Then the solution was heated at 200°C for 48 h in autoclave. Finally, the $Ag_{0.4}V_2O_5$ nanobelts were received [57]. The microstructure results and the XRD pattern as shown in Figure 17, the phase $Ag_{0.4}V_2O_5$ is a monoclinic structure.

To study the electrochemical properties of Zn //$Ag_{0.4}V_2O_5$ battery, the cyclic voltammetry curve (CV) at scan rate 0.1 mV·s^{-1} start from 0.4 V to 1.4 V, three reduction peaks occurring as shown in Figure 18. The first 5 cycles show that the capacity quickly decreases but then becomes stable after 5 cycles. The cycle performance shows a high capacity of 225 mAh·g^{-1} at the current density of 5 A·g^{-1} after 1000 cycles and it can still maintain a stable capacity of 144 mAh·g^{-1} at the current density of 10 A·g^{-1} after 2000 cycles [57].

The $Ag_{0.4}V_2O_5$ is a high-efficiency cathode material for aqueous ZIBs with great electrochemical performance, especially the long-term cycle stability at high current density. The silver networks in this cathode can increase the electrical conductivity of V_2O_5 to receive high performance cathode material.

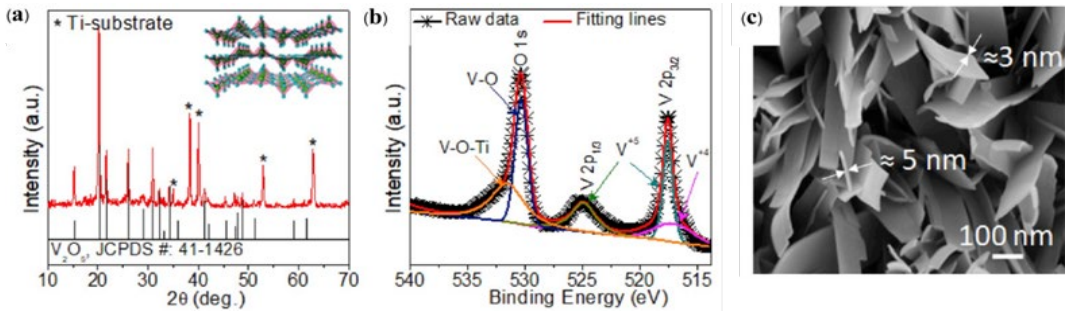

Figure 15. (a) XRD pattern, (b) XPS spectrum, and (c) FESEM images of V_2O_5 nanosheets growth directly on Ti-foil [56].

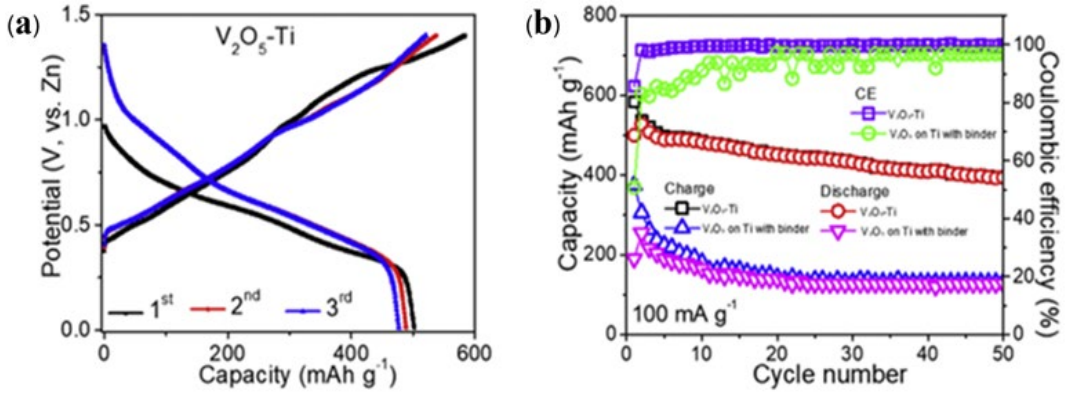

Figure 16. (a) Charge-discharge curves of first 3 cycles of V_2O_5-Ti, and (b) cycling ability of V_2O_5-Ti compared with V_2O_5-Ti-binder [56].

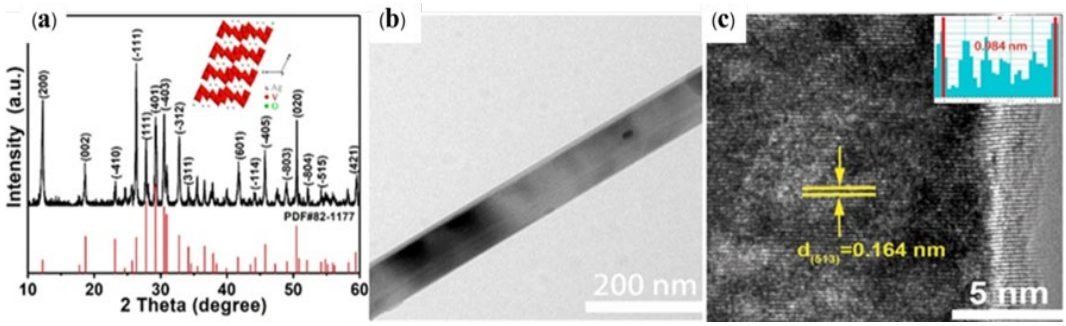

Figure 17. (a) XRD pattern, (b) TEM image and (c) HRTEM of $Ag_{0.4}V_2O_5$ nanobelts [57].

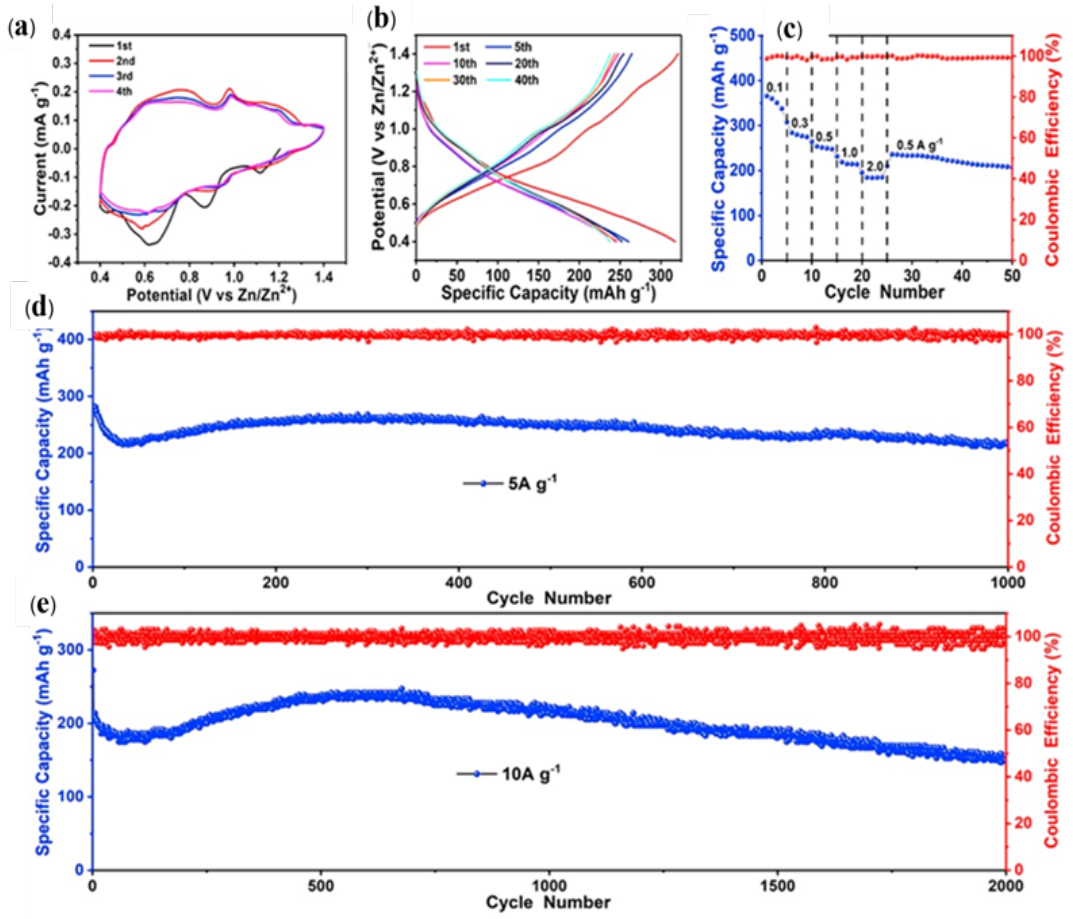

Figure 18. (a) CV curves, (b) the charge-discharge curves at current density 0.5 A·g^{-1}, (c) the rate performance, and (d,e) the cycle ability at 5 A·g^{-1}, and 10 A·g^{-1} of $Ag_{0.4}V_2O_5$ [57].

The sol–gel method is a simple process by Ni-doped V_2O_5 nanoparticles [58] can synthesized by this method. Finally, the blue gel was calcined at 400°C for 4 h and then V_2O_5 yellow powder was received. XRD and SEM were used to characterize morphologies and microstructure from XRD pattern showing the orthorhombic V_2O_5 structure, the SEM image presents the shape as like a nanorod size in a range of 60 nm to 80 nm and has a few non-uniforms distribution of Ni placed on V_2O_5 based surface displayed in the Figure 19.

From the CV curve, Ni-doped V_2O_5 shows a wider curve than pure V_2O_5 because Ni content in V_2O_5 nanorod can enhance the conducting of the material resulting in Ni-doped V_2O_5 electrode having a higher specific capacity than a normal V_2O_5 electrode. This material can be promoted as a new cathode material for Zinc ion batteries

This research group [59], report a cathode material for a zinc battery cell that is $Zn_{0.25}V_2O_5{\cdot}nH_2O$, with high a capacity ~300 $mAh{\cdot}g^{-1}$ and retention more than 80% over 1,000 cycles. By this cathode were synthesis by traditional hydrothermal processing resulting in superlong $Zn_{0.25}V_2O_5{\cdot}nH_2O$ nanobelts with lattice spacing 0.537 nm distance of the (200) planes were obtained the morphology were investigated as shown in Figure 21.

Figure 22 presents a schematic of the rechargeable ZIB by Zn metal as an anode, $Zn_{0.25}V_2O_5$ as a cathode in an aqueous 1 M $ZnSO_4$ system. During the charge-discharge process, it incorporation water molecule and V_2O_5 layer resulting in interlayer arrangement of each layer was expand to obtain a high capacity of 250 $mAh{\cdot}g^{-1}$ at 1.2 $A{\cdot}g^{-1}$ with a long cycle stability over 200 cycles [59].

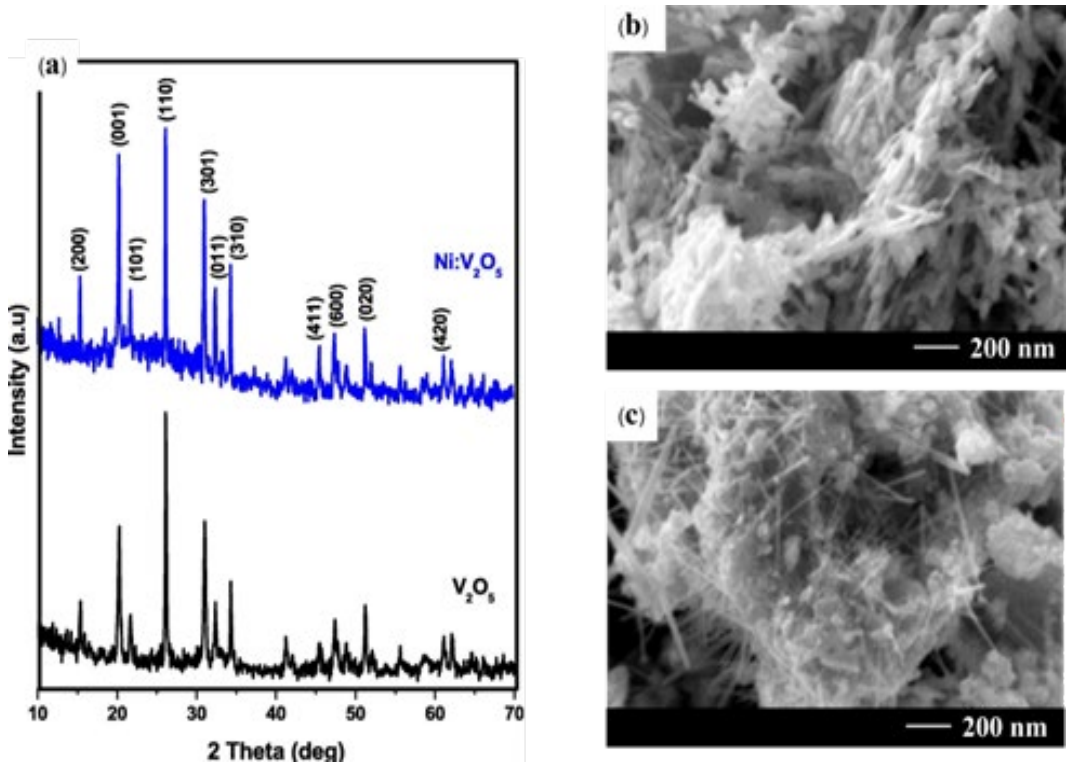

Figure 19. XRD spectra and SEM images of (a) pure V_2O_5, and (b) Ni-doped V_2O_5 [58].

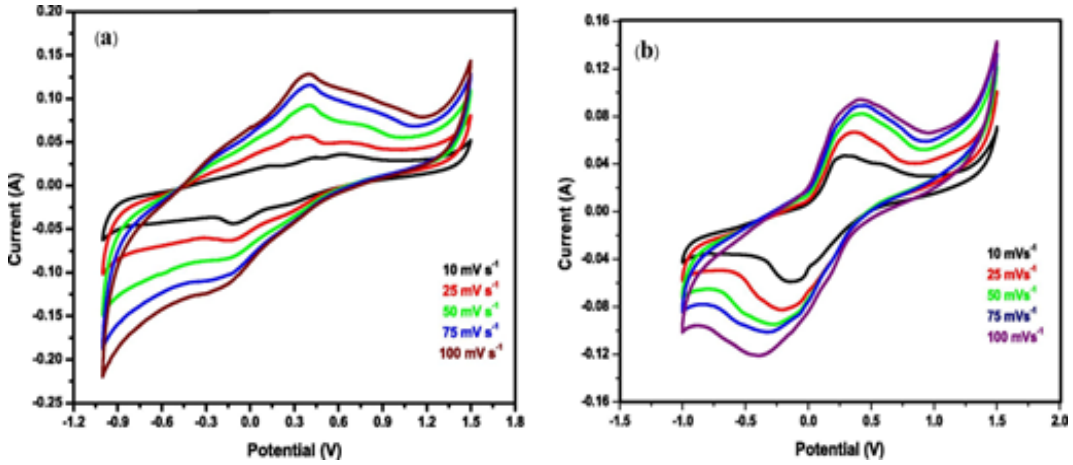

Figure 20. CV curves of (a) pure V_2O_5, and (b) Ni-doped V_2O_5 [58].

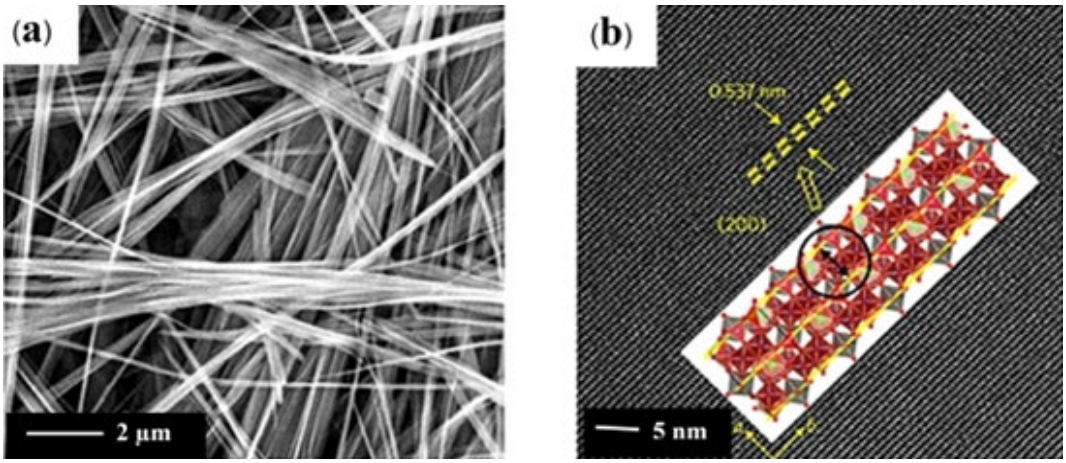

Figure 21. (a) SEM image, and (b) HRTEM image of $Zn_{0.25}V_2O_5{\cdot}nH_2O$ nanobelts [59].

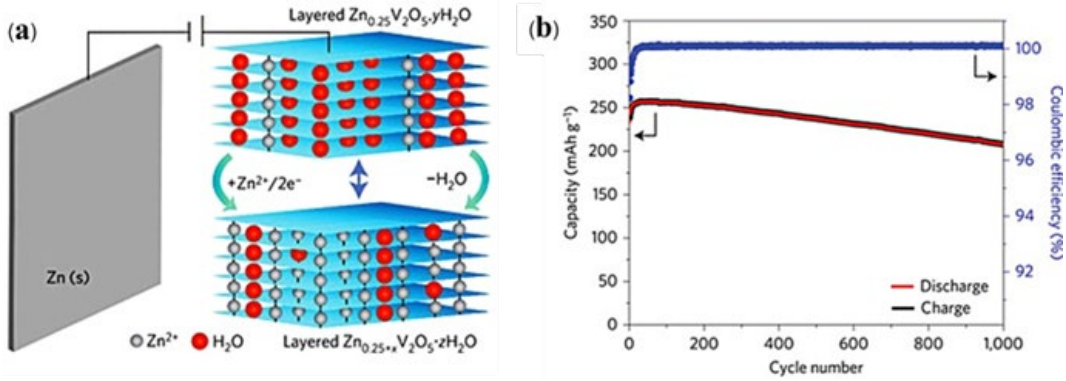

Figure 22. (a) A schematic, and (b) cycle performance of Zn // $Zn_{0.25}V_2O_5$ [59].

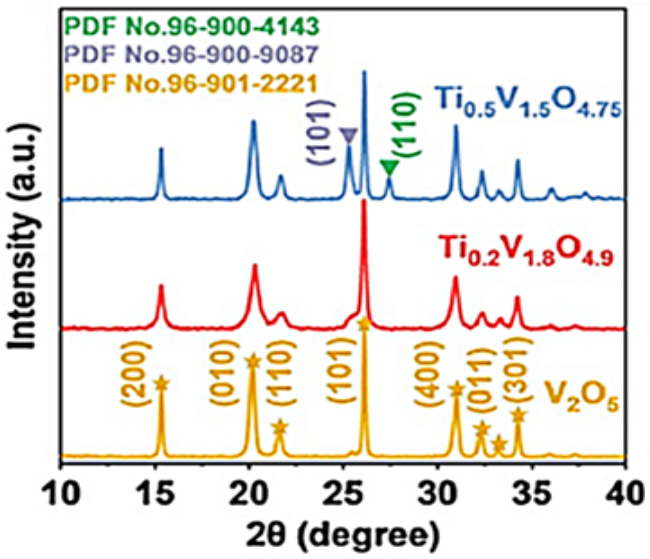

Figure 23. XRD spectrum of $Ti_{0.2}V_{1.8}O_{4.9}$ and $Ti_{0.5}V_{1.5}O_{4.75}$[60].

The Ti-doped V_2O_5 can be prepared from the simple spray-drying method and annealing in the muffle furnace at 400°C with an aging time of 2 h by various Ti content and V content then obtained $Ti_{0.2}V_{1.8}O_{4.9}$ as called TVO [60]. These materials confirmed the structure by XRD as displaying the V_2O_5 spectrum, orthorhombic phase. Figure 24 is SEM image of V_2O_5 presents porous spherical with a size of 50 nm to 100 nm under layer can observe porous yolk. Both $Ti_{0.2}V_{1.8}O_{4.9}$ and $Ti_{0.5}V_{1.5}O_{4.75}$ are the yolk-shell microspheres without mesopores on the surface also has Ti uniform distribution that can confirm the complete Ti doping in V_2O_5.

The electrochemical performance used to study the effect of Ti doping in V_2O_5 was prepared a coin cell CR2025 with 3M $ZnSO_4$ as the electrolyte. The cyclic voltammetry (CV) curves at scan rate 0.1 $mV{\cdot}s^{-1}$ show that both $Ti_{0.2}V_{1.8}O_{4.9}$ and $Ti_{0.5}V_{1.5}O_{4.75}$ occur a pair of the reduction reaction peaks as shown in Figure 25. $Ti_{0.2}V_{1.8}O_{4.9}$ has a higher capacity than $Ti_{0.5}V_{1.5}O_{4.75}$ when compared the cycle ability at current density 1 $A{\cdot}g^{-1}$ also higher with 89% capacity retention after 2500 cycles.

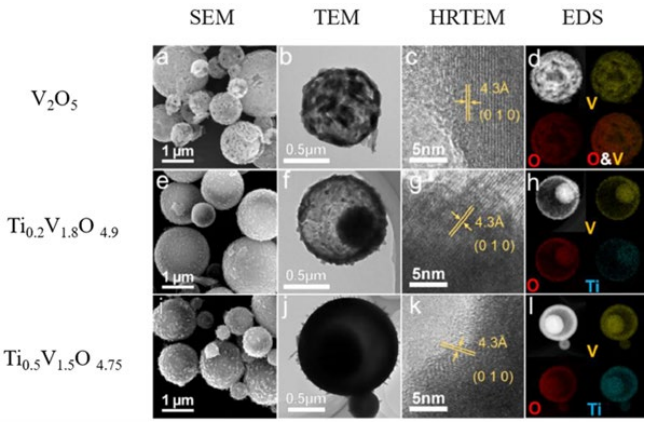

Figure 24. The microstructure of V_2O_5, $Ti_{0.2}V_{1.8}O_{4.9}$ and $Ti_{0.5}V_{1.5}O_{4.75}$ [60].

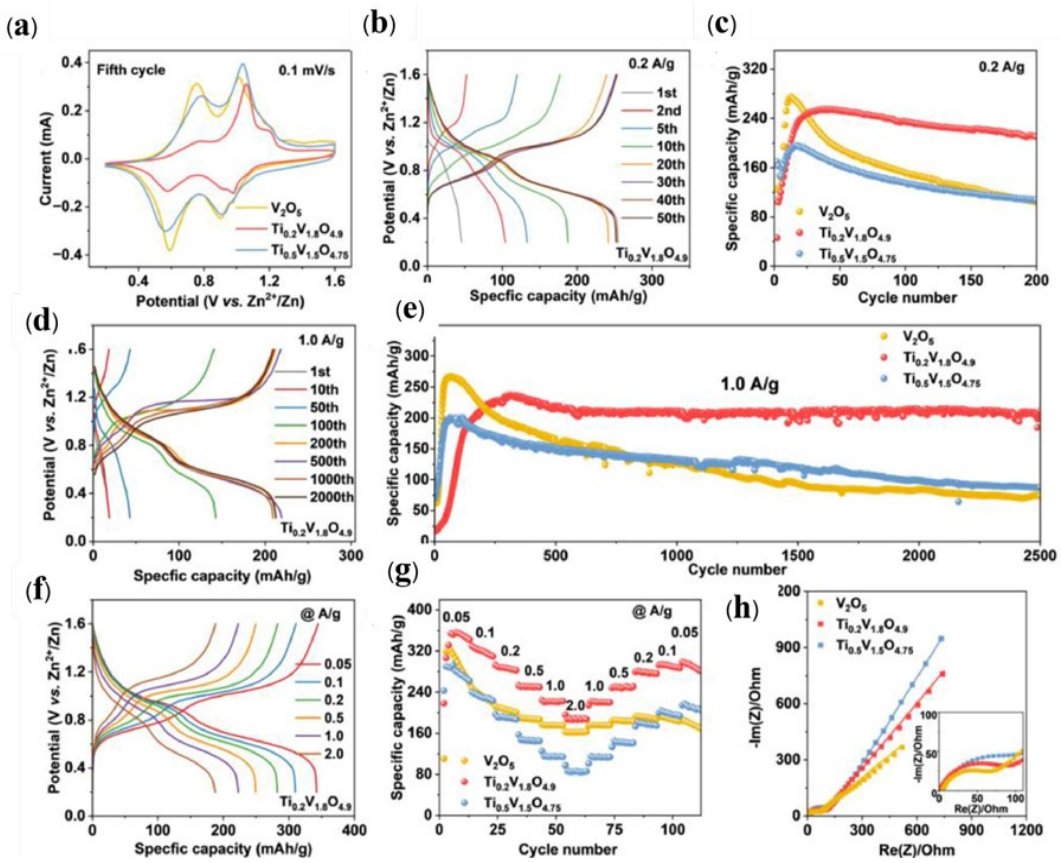

Figure 25. (a) The 5th cycle CV profile of V_2O_5, $Ti_{0.2}V_{1.8}O_{4.9}$ and $Ti_{0.5}V_{1.5}O_{4.75}$, (b) GCD profiles of $Ti_{0.2}V_{1.8}O_{4.9}$, (c) Cycling ability at 0.2 $A{\cdot}g^{-1}$, (d) GCD curves of $Ti_{0.2}V_{1.8}O_{4.9}$ at 1.0 $A{\cdot}g^{-1}$, (e) Cycling ability at 0.2 $A{\cdot}g^{-1}$. (f) GCD curves of $Ti_{0.2}V_{1.8}O_{4.9}$, (g) Rate performances of V_2O_5, $Ti_{0.2}V_{1.8}O_{4.9}$ and $Ti_{0.5}V_{1.5}O_{4.75}$, and (h) EIS plots of V_2O_5, $Ti_{0.2}V_{1.8}O_{4.9}$ and $Ti_{0.5}V_{1.5}O_{4.75}$ [60].

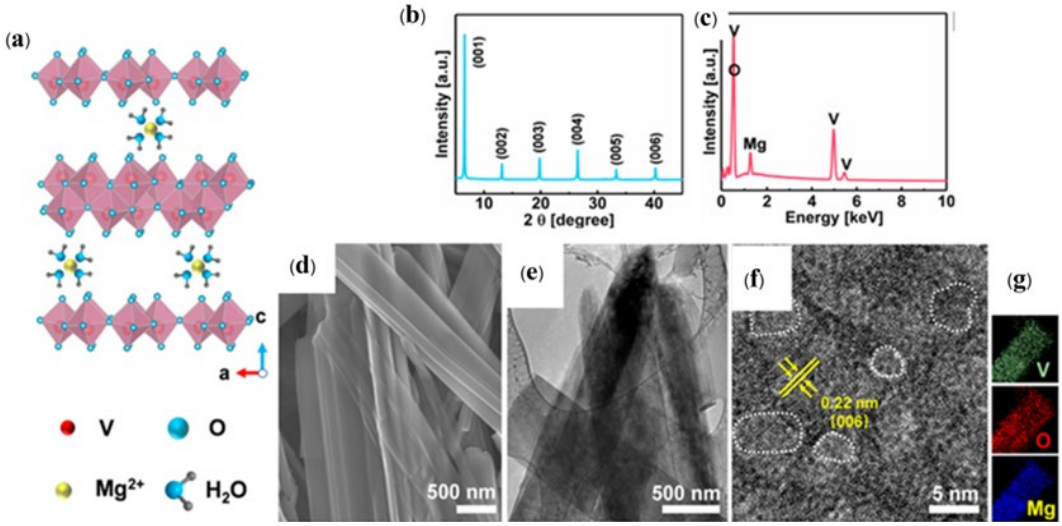

Figure 26. Structural characterization of MVO cathodes. (a) crystal structure, (b) XRD pattern, (c) EDS spectrum, (d-f) SEM, TEM, HRTEM images, and (g) TEM-EDS elemental maps [61].

Transition metal doping (Ti) can reduce the solubility of cathode material in aqueous electrolytes and can improve the long-term stability of the battery. Ming F. *et al.* reported a porous $Mg_{0.34}V_2O_5{\cdot}0.84H_2O$ nanobelts (MVO) were synthesized by hydrothermal method at a temperature 220°C for 48 h [61]. The structure was investigated by XRD as confirmed $V_2O_5{\cdot}0.5H_2O$, SEM was used to study morphology, TEM and HRTEM to analyze lattice spacing and element mapping the result as shown in Figure 26. The morphology of MVO is the nanobelts ~10 μm in length and ~500 nm in width and can see a porous surface with a lattice spacing ~ 0.22 nm. To prove the element of MVO nanostructure has Mg, V and O elements via use of TEM-EDS mapping can observe the uniform distribution of each element. These results prove this method can produce porous layered MVO [61] .

For electrochemical measurements, the AZIBs were prepared, the CV profile at scan rate 0.2 $mV \cdot s^{-1}$ displays the operating voltage window from 0.1 V to 1.8 V, it is larger than previous reports.

Figure 27 shows the rate performance of MVO at different current densities from 0.05 $A \cdot g^{-1}$ to 5 $A \cdot g^{-1}$ and then backward to 0.1 $A \cdot g^{-1}$ with the discharge capacity ~350 $mAh \cdot g^{-1}$ at 0.05 $mA \cdot g^{-1}$ when backward to 0.1 $A \cdot g^{-1}$ still high capacity ~330 $mAh \cdot g^{-1}$with capacity retention ~97%. Thus, can confirm the long-term stability of this cathode that owing to Mg can provide large interlayer spacing and the concentration of this electrolyte, $Zn(CF_3SO_3)_2$ has more acidic than $ZnSO_4$, resulting in oxygen evolution reaction (OER) kinetics reaction is lower and can improve to higher capacity and energy density than normal $ZnSO_4$.

The hydrothermal add-on annealing can used to prepare $Cu_{0.1}V_2O_5 \cdot 0.08H_2O$ to adjust the crystalline structure by synthesizing at 200°C for 48 h. After that further annealing by various temperatures from 100°C to 600°C in the air [62] when the annealing temperature is nearly 300°C presented water molecules almost evaporate. So, the CuVO-300 composite has a chemical formula is $Cu_{0.1}V_2O_5 \cdot 0.08H_2O$ which is an optimized parameter. The microstructures were observed by SEM, XRD and TEM to measure the copper (Cu) content in vanadium (V), the result is shown in Figure 28.

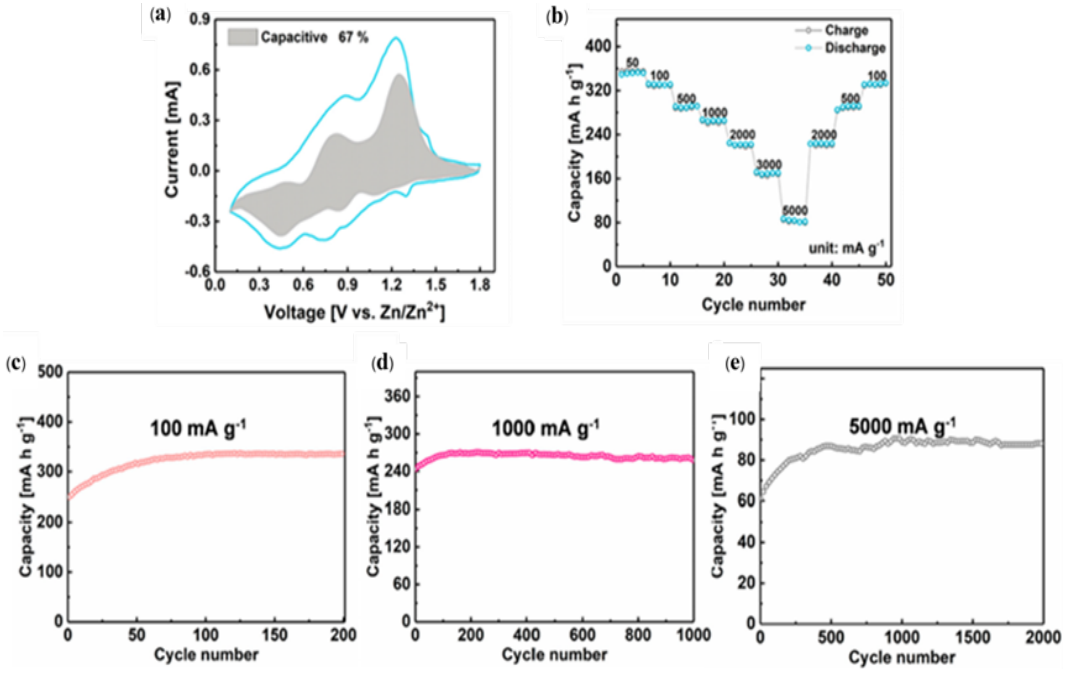

Figure 27. (a) The CV profile, (b) rate performance various current density, and (c-e) cycle performances at current densities 0.1, 1, and 5 $A \cdot g^{-1}$ [61].

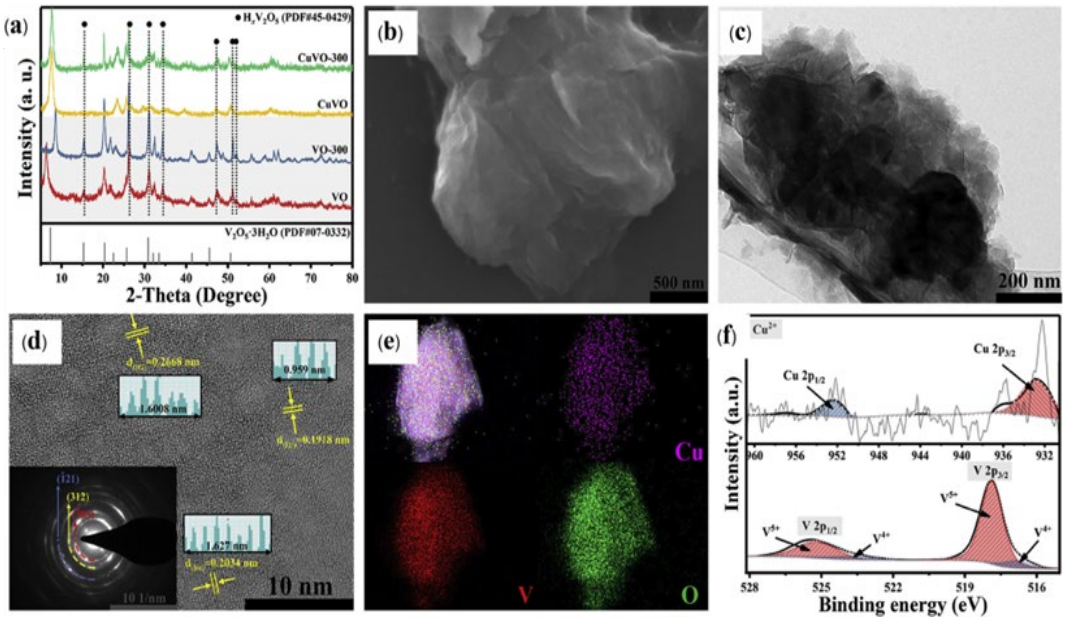

Figure 28. (a) XRD spectrum, (b,c) SEM and TEM image, (d) HRTEM image, (e,f) TEM-EDX and XPS spectra of the CuVO-300 composite [62].

To study the electrochemical performance, the coin cells (CR2016) were prepared, the cyclic voltammetry profile of CuVO-300 at a scan rate of 0.1 $mV \cdot s^{-1}$ display 3 pair of the reduction peak as shown in Figure 29 in range of 0.4 V to 1.3 V. The cycle performance as show high capacity ~350 $mAh \cdot g^{-1}$ at current density 1 $A \cdot g^{-1}$ which higher than normal V_2O_5 because of pure V_2O_5 its narrow layer spacing and low conductivity. Adding metal ions into the V_2O_5 interlayers increases the structural stability during cycling but also including enhance the interlayer spacing to a large size affected on has a higher electrical conductivity that and can apply to other cathode materials or battery system.

FeVO and VO nanobelts were synthesized using a single-step hydrothermal method via with and without doping elements [63]. The schematic illustration of the preparation method is shown in Figure 30 this Fe-doped material creates a new pathway for zinc ion movement and also a stable layered structure with significantly increased layer spacing up to 10.8 Å.

Figure 31 presents a comparison between commercial V_2O_5 and FeVO, the FeVO shows a diffraction peak at 2θ of 8.17° with (001) plane has a lattice spacing of 10.8 Å indicating the expands layer distance which supported Zn^{2+} ions diffusion into each layer. FESEM and HRTEM were used to characterize the morphology and structure of these materials. The SEM images show FeVO nanobelt structure with the uniform distribution of V, O and Fe in a range of 20 nm to 150 nm, similar to the pure VO. The (201) plane of FeVO with the interspacing 0.46 nm.

The electrochemical properties was tested in a CR2032 coin cell, CV profiles at a scan rate of 0.1 $mV \cdot s^{-1}$ of the first 5 cycles of FeVO shown in Figure 32 with an operating window of 0.2 V to 1.6 V these observed 3 pairs of redox peaks suggest that zinc ions (Zn^{2+}) are insertion and extraction from the FeVO are the multi-step reaction. The reversible electrochemical behavior of the FeVO is shown on the high CV peak which is the effect of Fe doping.

The initial resistance (Rct) of the FeVO is lower than the pure VO and commercial V_2O_5. This is quite high at 2189 Ω, but this resistance significantly drops after the first, 50th, and 100th cycles due to an electrochemical activation process. At a low current of 0.2 $A \cdot g^{-1}$, the FeVO exhibits a specific capacity of 276.2 $mAh \cdot g^{-1}$ and capacity retention of 93.6% after 150 cycles and also at a higher current density of 0.5 $A \cdot g^{-1}$ and then compared with another cathode this cathode displays longer cycle stability than the pure VO and commercial V_2O_5 with a specific capacity of 236.2 $mAh \cdot g^{-1}$ and capacity retention of 94.6% after 300 cycles. The high structural stability FeVO presents a higher capacity than those of VO and V_2O_5 owing to the Fe doping an expanded layer spacing promotes ion diffusion. This dopant improves the ability to charge and discharge toward high capacity and long-term cycle stability.

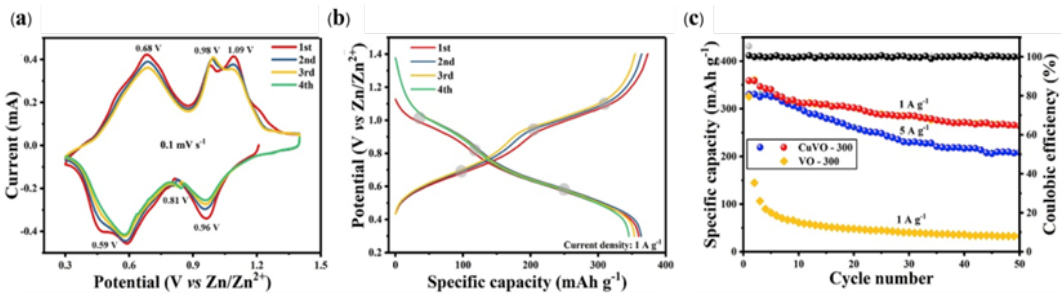

Figure 29. (a) CV curves, (b) GCD profile of CuVO-300 at 1 $A \cdot g^{-1}$, and (c) cycling performances the CuVO-300 composite [62].

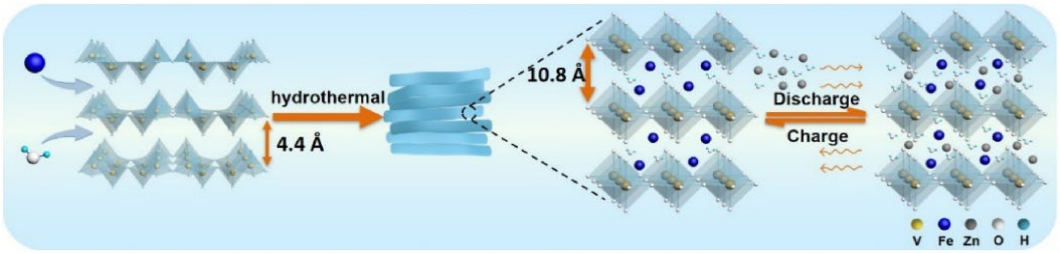

Figure 30. Schematic illustration preparation method and the model of Fe-doped VO [63].

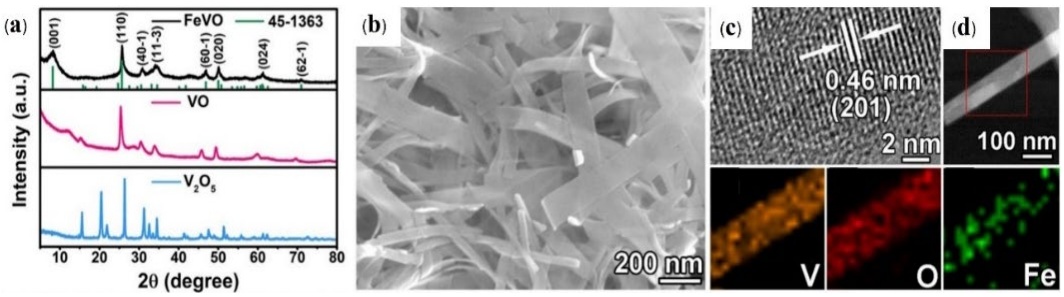

Figure 31. Structural and morphology analysis (a) XRD patterns of all materials compared to commercial V_2O_5, (b) SEM image, (c) HRTEM image, (d) elemental mapping of FeVO [63].

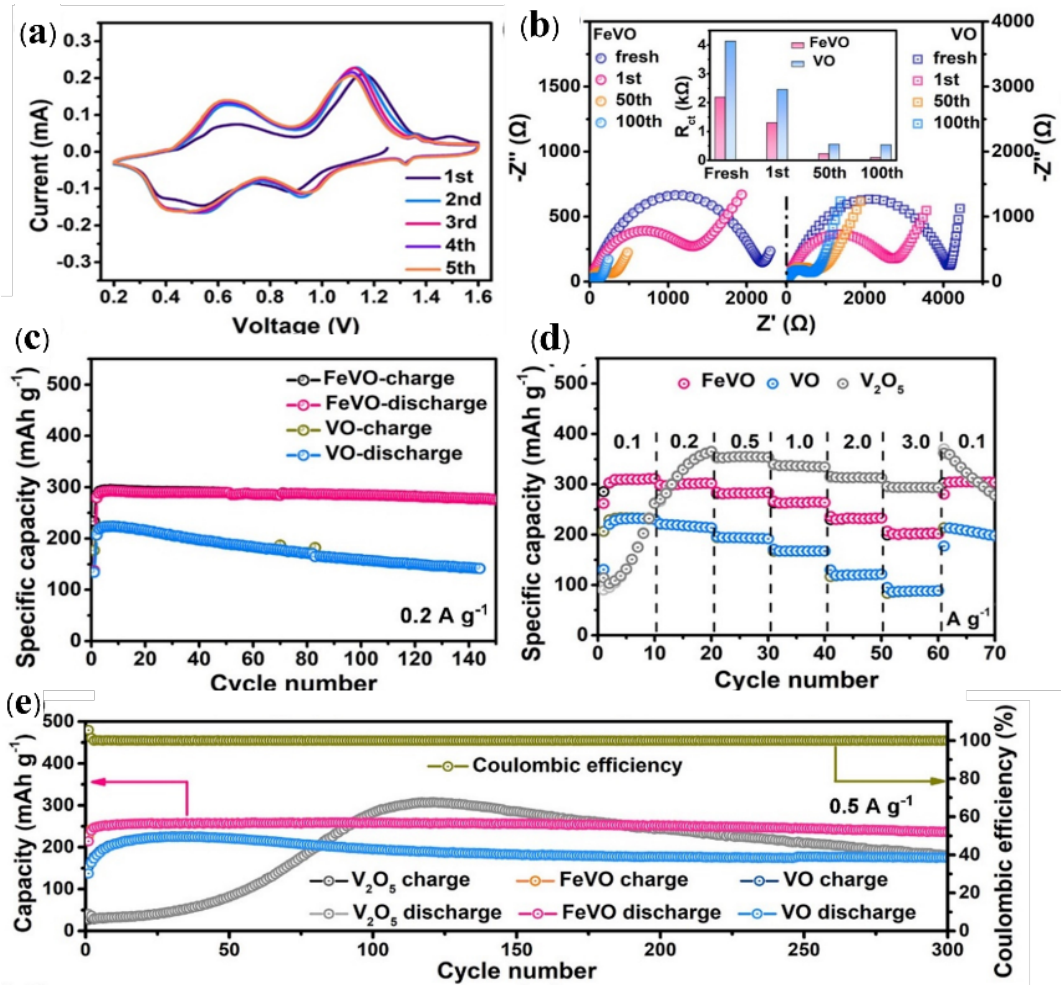

Figure 32. (a) CV profile of FeVO, (b) the Nyquist plots of FeVO and pure VO, (c) Cycling performance at 0.2 $A \cdot g^{-1}$, (d) rate performance, and (e) cycling performance at 0.5 $A \cdot g^{-1}$ [63].

This study uses a simple one-step hydrothermal method that involves varying the ratios of Cu and V_2O_5 to produce Cu pre-intercalated into V_2O_5, which is a composite phase of $Cu_{0.4}V_2O_5$ consisting of copper vanadate and zinc vanadate were mixing and $VO_2 \cdot nH_2O$ nanosheets that with the chemical formula $(Cu_{0.4}V_2O_5)_x \cdot (VO_2 \cdot nH_2O)_y$ [64]. The schematic describes the synthesis method, as shown in Figure 33. The XRD, SEM, and EDS mapping images, TEM, and high-resolution TEM (HRTEM) were used. Figure 34 displays the SEM analysis with a uniform distribution of Cu, V, and O nanosheets with a width of 70 nm to 160 nm, 200 nm to 500 nm length and an average thickness of 22 nm. The TEM images showed a layered structure with a d-spacing of 0.368 nm and an interlayer distance of 9.125 Å, much larger than the previously reported.

The electrochemical performance was evaluated by assembling CR2032-type coin cells. The CV curve at scan rates of 0.1 $mV \cdot s^{-1}$ to 1 $mV \cdot s^{-1}$ Figure 35 exhibited consistent shapes, with reduction and oxidation peaks shifting towards the left and right when the scan rates increased. This suggests high rate performance. The result shows this material has an impressive highest reversible capacity of 292 $mAh \cdot g^{-1}$, with 91% retention and exhibits long-term performance at high current density with a capacity of 332 $mAh \cdot g^{-1}$ at 0.2 $A \cdot g^{-1}$ in the voltage range of 0.3 V to 1.6 V.

The batteries performance is enhanced by the phase change of Cu and Zn vanadate as well as the reversible redox reactions of Cu^{2+} and Cu^0 by increasing the distance between layers with the high conductivity leading to a high Zn ions diffusion rate.

The development of Ni-doped V_2O_5@3 D Ni core/shell composites on a carbon cloth electrode by forming Ni-V_2O_5 on free-standing 3D Ni metal nanonets [65]. The schematic of the preparation process of these materials was explained in the Figure 37. The Ni doping can enhance the interlayer spacing of V_2O_5 which can expand the operating window (0.3 V to 1.8 V) and the zinc-ion reaction kinetics that allow fast Zn^{2+} ion transport. In this work, the one-step loading process mixed Ni particles from 3D nanonets into V_2O_5 via hydrothermal and annealed in air at 300°C, which changed the structure of the layers between the active materials. To investigate the structure and morphology, SEM and XRD were used to characterize. Figure 33(d,e) After low-temperature annealing, rod-shaped 3D nanosheets on CC was obtained. The homogeneous distribution of V_2O_5 nanosheets on the surfaces of the 3D Ni nanonets displays in Figure 33(f,g) form unique core-shell composites. The XRD and XPS confirm that has Ni-incorporated V_2O_5. Between each layer has Ni incorporated effect on the structural and the electronic environment of V and O causing shifts in the binding energies.

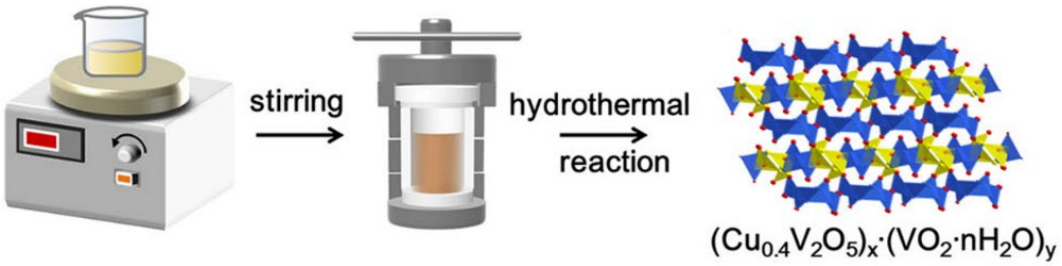

Figure 33. Schematic of the synthesis of $(Cu_{0.4}V_2O_5)_x \cdot (VO_2 \cdot nH_2O)_y$ nanosheets [64].

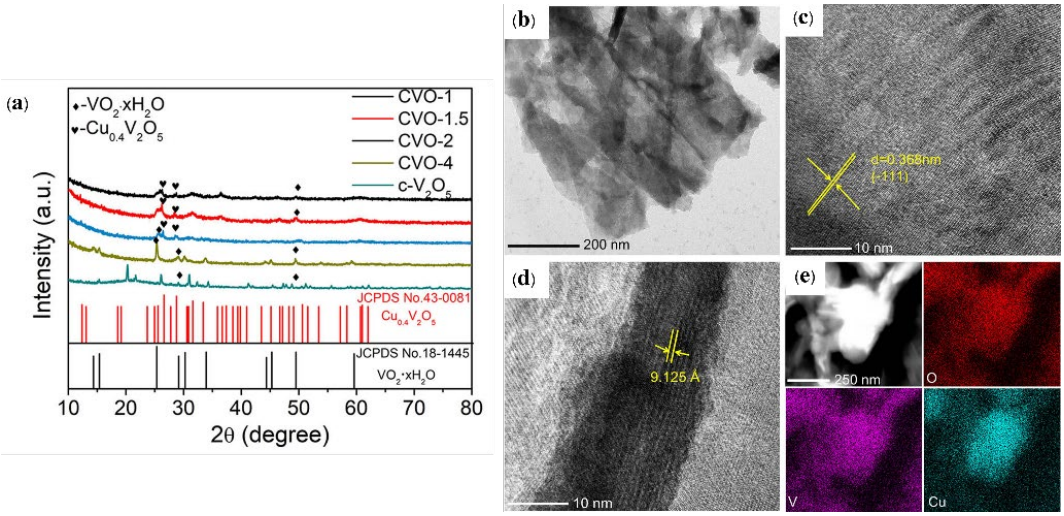

Figure 34. (a) The XRD patterns of all materials, (b) TEM image, (c-d) HRTEM image, (e) SEM image and elemental mappings of V, O, and Cu of CVO-2 [64].

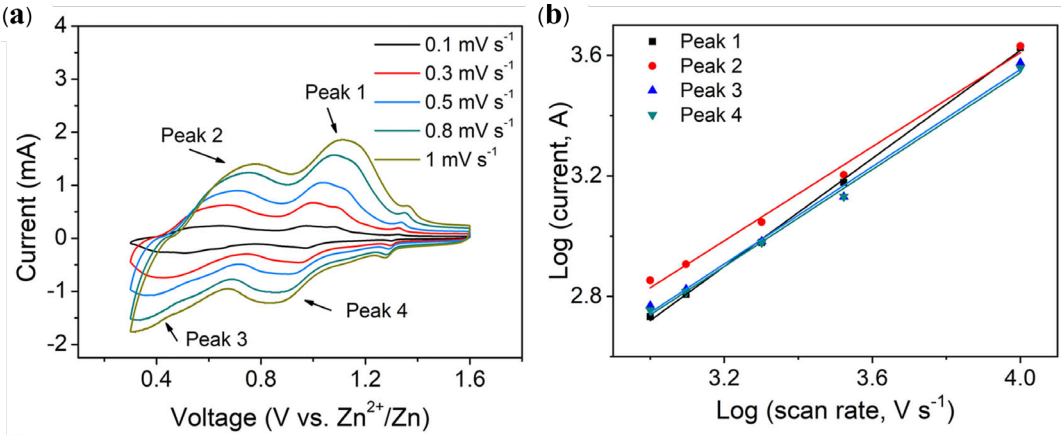

Figure 35. CV curves, (b) log(i) vs log(v) plots in CV curves of CVO-2 [64].

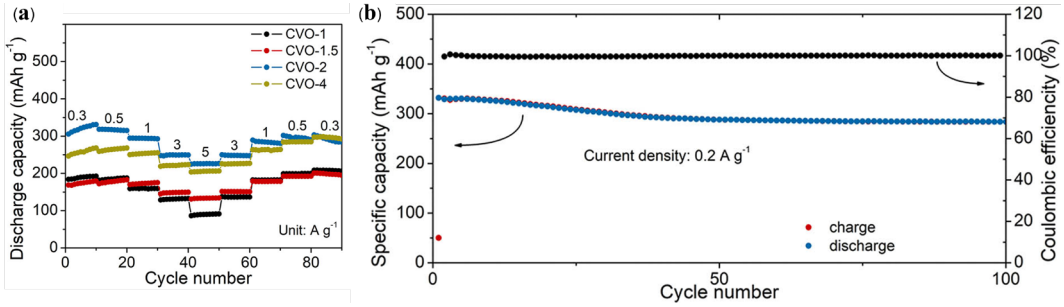

Figure 36. (a) rate performance of all materials, and (b) cycle ability of CVO-2 at 0.2 A·g^{-1} [64].

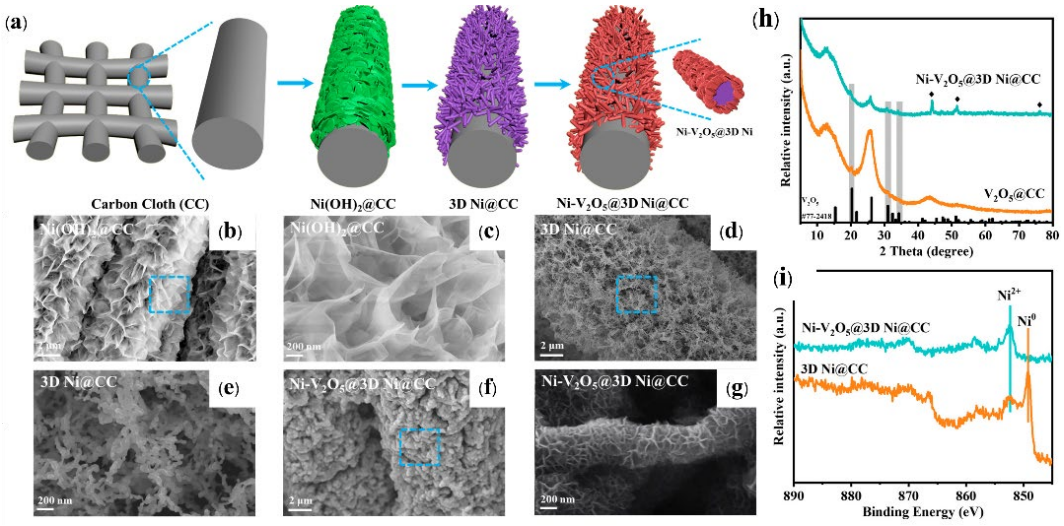

Figure 37. (a) The schematic of the preparation process, SEM images of (b,c) $Ni(OH)_2$ nanosheets on CC, (d,e) 3D Ni nanonets on CC, (f,g) Ni- V_2O_5@3D Ni@CC, and (h,i) XRD and XPS spectra of these materials [65].

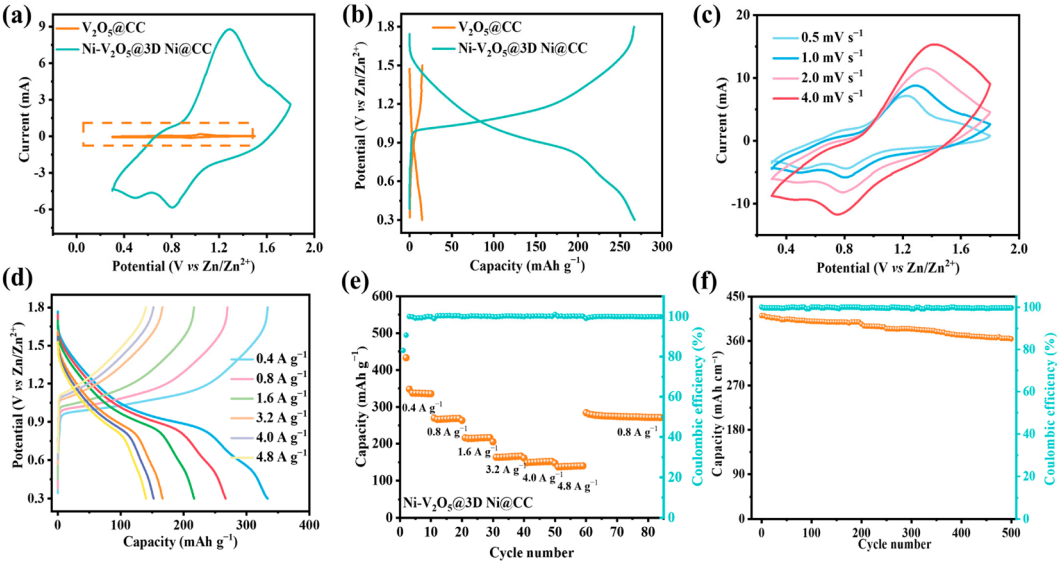

Figure 38. (a) CV profile of V_2O_5@CC and Ni- V_2O_5@3D Ni@CC, (b) GCD curves of V_2O_5@CC and Ni- V_2O_5@3D Ni@CC at current density of 0.8 $A \cdot g^{-1}$, (c) CV profile of Ni- V_2O_5@3D Ni@CC at various scan rates from 0.5 $mV \cdot s^{-1}$ to 4.0 $mV \cdot s^{-1}$,(d) GCD curves of Ni- V_2O_5@3D Ni@CC at various current densities, (e) rate capability test of Ni- V_2O_5@3D Ni@CC various current, and (f) cyclability of Ni- V_2O_5@3D Ni@CC at a current density of 4.8 $A \cdot g^{-1}$ [65].

Table 1. The summary of synthesis method and electrochemical performances of recently reported metals doping V_2O_5 for AZIBs.

Materials	Method	Electrolyte	Specific capacity ($mAh \cdot g^{-1}$)	Current density ($A \cdot g^{-1}$)	Retention % (cycles)	Ref.
$Co_{0.247}V_2O_5 \cdot 0.944H_2O$	hydrothermal	21M LiTFSi + 1M $Zn(CF_3SO_3)_2$	450	4	90.26 (7,500)	[55]
2D V_2O_5-Ti	hydrothermal	3 M $Zn(CF_3SO_3)_2$	503.1	0.1	98 (50)	[56]
$Ag_{0.4}V_2O_5$	hydrothermal	3M $ZnSO_4$	237	0.5	85 (1,000)	[57]
Ni-doped V_2O_5	Sol-gel	2 M $ZnSO_4$	-	-	-	[58]
$Zn_{0.25}V_2O_5 \cdot nH_2O$	hydrothermal	3M $ZnSO_4$	300	0.05	80 (2,000)	[59]
$Ti_{0.2}V_{1.8}O_{4.9}$	hydrothermal	3M $ZnSO_4$	355	0.05	89 (2,500)	[60]
$Mg_{0.34}V_2O_5 \cdot 0.84H_2O$	hydrothermal	3M $Zn(CF_3SO_3)_2$	350	0.05	97 (1,000)	[61]
$Cu_{0.1}V_2O_5 \cdot 0.08H_2O$	hydrothermal	2M $ZnSO_4$	359	1.0	88 (1,000)	[62]
FeVO	hydrothermal	3M $Zn(CF_3SO_3)_2$	236.2	0.5	94.6 (300)	[63]
$Cu_{0.4}V_2O_5 \cdot (VO_2 \cdot nH_2O)_y$	hydrothermal	1.8M $Zn(CFSO_3)_2$	332	0.2	97 (100)	[64]
Ni-V_2O_5@3D Ni@CC	hydrothermal	2M $ZnSO_4$	405	4.8	98 (500)	[65]

The electrochemical properties were studied and the result as shown in Figure 38. Cyclic voltammetry (CV) was measured at a scan rate of 1.0 $mV \cdot s^{-1}$ compared to the pure V_2O_5@CC and the Ni-V_2O_5 @3D Ni@CC this shows a wider voltage window of 0.3 V to 1.8 V enables to work at a high energy density and also the GCD profile provides a higher capacity of 270 $mAh \cdot g^{-1}$ at the current density of 0.8 $A \cdot g^{-1}$ due to its high specific surface area and electrical conductivity. Moreover, at a higher current density of 4.8 $A \cdot g^{-1}$, after cycling over 500 times this material is still almost 100% CE. The 3D framework Ni nanonets are better than CC because they have a larger surface area and better electrical conductivity.

The 3D Ni nanonet can intercalate to active material as an incorporation ion into the layer V_2O_5 could not only serve as a framework but could also alter the V_2O_5 internal layer structure, promoting ion and electron transport and accelerating the oxidation-reduction process resulting in a higher energy density and ion transfer rate while maintaining long-term stability.

4. Summary and outlook

However, vanadium-based compounds display challenges as the same Mn-based materials and Prussian blue analogs, presenting fading long-term cycle stability due to V-based electrode materials having poor electrical conductivity and unstable structure can change to some failure structure which a narrow layer spacing and high dissolution in electrolytes during the charge and discharge mechanism, results in low working potential, with low cycle stability and energy density.

This mini review summarizes some transition metal doping in V_2O_5 this is one of several methods that can solve the limitation of V-based cathode materials for aqueous zinc-ion batteries (AZIBs) to increase electrical conductivity and dopant atoms can inserted between each interlayer to receive large interlayer spacing as compared to with the commonly V_2O_5, Including can also enhance the cathode performance for high capacity and long cycle stability that can be developing AZIBs to large scale applications. The vanadium-based cathodes are promising good candidate for high-performance zinc-ion batteries due to their unique properties. Their diverse structural configurations and multiple oxidation states offer significant potential for enhancing energy density and power capability. However, challenges such as conductivity, vanadium dissolution, and cycle life stability require further investigation. To unlock the full potential of vanadium oxide cathodes, future research should focus on optimizing structure, composite engineering, and developing electrolyte formulations. Additionally, in-depth studies on reaction mechanisms and degradation processes are essential for improving battery lifespan and safety. By addressing these areas, vanadium-based zinc-ion batteries can be positioned as a viable and sustainable energy storage solution for the future.

Acknowledgment

J. Cao would like to thank the support from Hubei Provincial Natural Science Foundation of China (Grant No. 2023AFB155). J. Qin would like to thank the Thailand Science Research and Innovation Fund Chulalongkorn University (INDF67620003), the National Science, Research and Innovation Fund (NSRF) via the Program Management Unit for Human Resources & Institutional Development, Research and Innovation (Grant no. B05F640153), and the National Research Council of Thailand (NRCT) and Chulalongkorn University (N42A660383).

References

[1] P. A. Owusu, and S. Asumadu-Sarkodie, "A review of renewable energy sources, sustainability issues and climate change mitigation," *Cogent Engineering*, vol. 3, no. 1, p. 1167990, 2016.

[2] X. Jia, C. Liu, Z. Neale, J. Yang, and G. Cao, "Active materials for aqueous zinc ion batteries: Synthesis, crystal structure, morphology, and electrochemistry," *Chemical Reviews*, vol. 120, no. 15, pp. 7795-7866, 2020.

[3] H. A. Kiehne, Battery technology handbook (2nd ed.). Engineering & Technology. 2003, Boca Raton: CRC Press. 542.

[4] B. Viswanathan, Chapter 12 - Batteries, in Energy Sources, B. Viswanathan, Editor. 2017, Elsevier: Amsterdam. p. 263-313.

[5] J. Cao, Y. Sun, D. Zhang, D. Luo, H. Wu, X. Wang, C. Yang, L. Zhang, X. Yang, and J. Qin, "Regulating Electrode/electrolyte interface with additives towards dendrite-free zinc-ion batteries," *ChemElectroChem*, vol. 11, no. 13, p. e202400064, 2024.

[6] J. Cao, X. Wang, D. Zhang, R. Chanojaree, L. Zhang, J. Qin, and X. Yang, "Boosting Zn metal anode stability with a dimethyl-formamide additive," *Journal of Alloys and Compounds*, vol. 972, p. 172773, 2024.

[7] U. E. Solutions , The Disadvantages of Lithium-Ion Batteries for Electric Cars, in EV charging, E.y. way, Editor. 2023: https://energy5.com/the-disadvantages-of-lithium-ion-batteries-for-electric-cars.

[8] J. Cao, J. Wu, H. Wu, Y. Jin, D. Luo, X. Yang, L. Zhang, D. Zhang, J. Qin, and J. Lu, "Dendrite-free Zinc anode via oriented plating with alkaline earth metal ion additives", *Advanced Functional Materials*, vol. 34, no. 32, p. 2401537, 2024.

[9] J. Cao, T. Ou, S. Geng, X. Zhang, D. Zhang, L. Zhang, D. Luo, X. Zhang, and J. Qin, "Constructing stable V_2O_5/V_6O_{13} hetero-structure interface with fast Zn^{2+} diffusion kinetics for ultralong lifespan zinc-ion batteries," *Journal of Colloid and Interface Science*, vol. 656, no. 12, p. 495-503, 2023.

[10] F. R. McLarnon, and E. J. Cairns, "The Secondary alkaline zinc electrode," *Journal of The Electrochemical Society*, vol. 138, no. 2, p. 645, 1991.

[11] J. Cao, D. Zhang, X. Zhang, M. Sawangphruk, J. Qin, and R. Liu, "A universal and facile approach to suppress dendrite formation for a Zn and Li metal anode," Journal of Materials Chemistry A, vol. 8, no. 18, p. 9331-9344, 2020.

[12] L. F. Arenas, A. Loh, D. Trudgeon, X. Li, C. P. de Leon, and F. C. Walsh, "The characteristics and performance of hybrid redox flow batteries with zinc negative electrodes for energy storage," *Renewable and Sustainable Energy Reviews*, vol. 90, p. 992-1016, 2018.

[13] J. Cao, D. Zhang, R, Chanajaree, X. Zhang, X. Yang, and J. Qin, "A low-cost separator enables a highly stable zinc anode by accelerating the de-solvation effect," *Chemical Engineering Journal*, vol. 480, p. 147980, 2024.

[14] T. Wang, C. Li, X. Xie, B. Lu, Z. He, S. Liang, and J. Zhou, "Anode Materials for aqueous zinc ion batteries: mechanisms,

properties, and perspectives," *ACS Nano*, vol. 14, no. 12, pp. 16321-16347, 2020.

[15] C. Xu, B. Li, H. Du, and F. Kang, "Energetic zinc ion chemistry: The rechargeable zinc ion battery," *Angewandte Chemie International Edition*, vol. 51, no. 4, pp. 933-935, 2012

[16] S. Islam, M. H. Alfaruqi, V. Mathew, J. Song, S. Kim, S. Kim, J. Jo, J. P. Baboo, D. T. Pham, D. Y. Putro, Y-K. Sun, and J. Kim, "Facile synthesis and the exploration of the zinc storage mechanism of β-MnO_2 nanorods with exposed (101) planes as a novel cathode material for high performance eco-friendly zinc-ion batteries," *Journal of Materials Chemistry A,* vol. 5, no. 44, pp. 23299-23309, 2017.

[17] M. H. Alfaruqi, V. Mathew, J. Gim, S. Kim, J. Song, J. P. Baboo, S. H. Choi, and J. Kim, "Electrochemically induced structural transformation in a γ-MnO_2 cathode of a high capacity zinc-ion battery system," *Chemistry of Materials*, vol. 20, no. 10, pp. 3609-3620, 2015.

[18] P. Senguttuvan, S-D. Han, S. Kim, A. L. Lipson, S. Tepavcevic, T. T. Fister, I. D. Bloom, A. K. Burrell, and C. S. Johnson, "A high power rechargeable nonaqueous multivalent Zn/V_2O_5 battery," *Advanced Energy Materials*, vol. 6, no. 24, p. 1600826, 2016.

[19] P. Hu, M. Yan, T. Zhu, X. Wang, X. Wei, J. Li, Z. Liang, Z. Li, L. Chen, and L. Mai, "Zn/V_2O_5 aqueous hybrid-ion battery with high voltage platform and long cycle life," *ACS Applied Materials and Interfaces,* vol. 9, no. 49, pp. 42717-42722, 2017.

[20] N. Zhang, Y. Dong, M. Jia, X. Bian, Y. Wang, M. Qiu, J. Xu, Y. Liu, L. Jiao, and F. Cheng, "Rechargeable aqueous Zn–V_2O_5 battery with high energy density and long cycle life," *ACS Energy Letters*, vol. 3, no. 6, pp. 1366-1372, 2018.

[21] J. Chen, G. Dawut, Y. Lu, and L Miao, "High-performance rechargeable aqueous Zn-ion batteries with a poly(benzoquinonyl sulfide) cathode," *Inorganic Chemistry Frontiers*, vol. 5, no. 6, pp. 1391-1396, 2018.

[22] J. Zhou, L. Shan, Z. Wu, X. Guo, F. Guozhao, and S. Liang, "Investigation of V_2O_5 as a low-cost rechargeable aqueous zinc ion battery cathode," *Chemical Communications*, vol. 54, no. 35, pp. 4457-4460, 2018.

[23] J. H. Jo, Y. K. Sun, and S. T. Myung, "Hollandite-type Al-doped $VO_{1.52}(OH)_{0.77}$ as a zinc ion insertion host material," *Journal of Materials Chemistry A*, vol. 5, no. 18, pp. 8367-8375, 2017.

[24] P. Y. Zavalij, F. Zhang, and M. S. Whittingham, "A new zinc pyrovanadate, $Zn_3(OH)_2V_2O_7.2H_2O$, from X-ray powder data," *Acta Crystallographica Section C: Crystal Structure Communications,* vol. 53, no. 12, pp. 1738-1739, 1997.

[25] B. Sambandam, V. Soundharrajan, S. Kim, M. H. Alfaruqi, J. Jo, S. Kim, V. Mathew, Y-K. Sun, and J. Kim, "Aqueous rechargeable Zn-ion batteries: An imperishable and high-energy $Zn_2V_2O_7$ nanowire cathode through intercalation regulation," *Journal of Materials Chemistry A*, vol. 6, no. 9, pp. 3850-3856, 2018.

[26] P. Hu, T. Zhu, X. Wang, X. Wei, M. Yan, J. Li, W. Luo, W. Yang, W. Zhang, Z. Liang, Z. Zhou, and L. Mai, "Highly durable $Na_2V_6O_{16}\cdot 1.63H_2O$ nanowire cathode for aqueous zinc-ion battery," *Nano Letters*, vol. 18, no. 3, pp. 1758-1763, 2018.

[27] X. Guo, F. Guozhao, W. Zhang, J. Zhou, L. Shan, L. Wang, C. Wang, T. Lin, Y. Tang, and S. Liang, "Mechanistic insights of Zn^{2+} storage in sodium vanadates," *Advanced Energy Materials*, vol. 8, no. 27, p. 1801819, 2018.

[28] B. Haüpler, C. Rossel, A. Schwenke, J. Winsberg, D. Korfer, A. Wild, and U. S. Schubert, "Aqueous zinc-organic polymer battery with a high rate performance and long lifetime," *NPG Asia Materials*, vol. 8, no. 7, p. e283, 2016.

[29] W. Kao-ian, A. A. Mohamad, W-R. Liu, R. Pornprasetsuk, S. Siwamogsatham, and S. Kheawhom, "Stability enhancement of zinc-ion batteries using non-aqueous electrolytes," *Batteries & Supercaps*, vol. 5, no. 5, p. e202100361, 2022.

[30] G. Li, Z. Yang, Y. Jiang, C. Jin, W. Huang, X. Ding, and Y. Huang, "Towards polyvalent ion batteries: A zinc-ion battery based on NASICON structured $Na_3V_2(PO_4)_3$," *Nano Energy*, vol. 25, pp. 211-217, 2016.

[31] S. D. Han, S. Kim, D. Li, V. Petkov, H. D. Yoo, P. Phillips, H. Wang, J. J. Kim, K. L. More, B. Key, R. F. Klie, J. Cabana, V. R. Stamenkovic, T. T. Fister, N. M. Markovic, A. K. Burrell, S. Tepavcevic, and J. T. Vaughey, "Mechanism of Zn insertion into nanostructured δ-MnO_2: A nonaqueous rechargeable Zn metal battery," *Chemistry of Materials*, vol. 29, no. 11, pp. 4874-4884, 2017.

[32] D. Kim, C. Lee, and S. Jeong, "A concentrated electrolyte for zinc hexacyanoferrate electrodes in aqueous rechargeable zinc-ion batteries" in IOP Conference Series: Materials Science and Engineering. 2018.

[33] K. E. K. Sun, T. K. A. Hoang, T. N. L. Doan, Y. Yu, and P. Chen, "Highly sustainable zinc anodes for a rechargeable hybrid aqueous battery," *Chemistry - A European Journal*, vol. 24, no. 7, pp. 1667-1673, 2018.

[34] K. E. K. Sun, T. K. A. Hoang, T. N. L. Doan, Y. Yu, X. Zhu, Y. Tian, and P. Chen, "Suppression of dendrite formation and corrosion on zinc anode of secondary aqueous batteries," *ACS Applied Materials and Interfaces*, vol. 9, no. 11, pp. 9681-9687, 2017.

[35] J. Cao, D. Zhang, C. Gu, X. Zhang, M. Okhawilai, S. Wang, J. Han, J. Qin, and Y. Huang, "Modulating Zn deposition via ceramic-cellulose separator with interfacial polarization effect for durable zinc anode," *Nano Energy*, vol. 89, p. 106322, 2021.

[36] G. Fang, J. Zhou, A. Pan, and S. Liang, "Recent advances in aqueous zinc-ion batteries," *ACS Energy Letters*, vol. 3, no. 10, p. 2480-2501, 2018.

[37] W. Lu, C. Xie, H. Zhang, and X. Li, "Inhibition of zinc dendrite growth in zinc-based batteries," ChemSusChem, vol. 11, no. 23, pp. 3996-4006, 2018.

[38] C. Zhai, D. Zhao, Y. He, H. Huang, B. Chen, X. Wang, and Z. Guo, "Electrolyte additive strategies for suppression of zinc dendrites in aqueous zinc-ion batteries," *Batteries*, vol. 8, no. 10, p. 153, 2022.

[39] T. Zhou, L. Zhu, L. Xie, Q, Han, X. Yang, L. Chen, G. Wang, and X. Cao, "Cathode materials for aqueous zinc-ion batteries: A mini review," *Journal of Colloid and Interface Science*, vol. 605, pp. 828-850, 2022.

[40] J. Cao, D. Zhang, R. Chanojaree, Y. Yue, Z. Zeng, X. Zhang, and J. Qin, "Stabilizing zinc anode via a chelation and desolvation electrolyte additive," *Advanced Powder Materials*, vol. 1, no. 1, p. 100007, 2022.

[41] J. Cao, D. Zhang, C. Gu, X. Wang, S. Wang, X. Zhang, J. Qin, and Z-S Wu, "Manipulating crystallographic orientation of zinc deposition for dendrite-free zinc ion batteries," *Advanced Energy Materials,* vol. 11, no. 29, p. 2101299, 2021.

[42] S. C. Pang, S. F. Chin, and C. Y. Ling, "Controlled synthesis of manganese dioxide nanostructures via a facile hydrothermal route," *Journal of Nanomaterials*, vol. 2012, no. 1, p. 607870, 2012.

[43] J. Cao, D. Zhang, X. Zhang, Z. Zeng, J. Qin, and Y. Huang, "Strategies of regulating Zn^{2+} solvation structures for dendrite-free and side reaction-suppressed zinc-ion batteries," *Energy & Environmental Science*, vol. 15, no. 2, pp. 499-528, 2022.

[44] M. Toupin, T. Brousse, and D. Bélanger, "Charge storage mechanism of MnO_2 electrode used in aqueous electrochemical capacitor," *Chemistry of Materials*, vol. 16, no. 16, pp. 3184-3190, 2004.

[45] Z. Wang, H. Tao, and Y. Yue, "Metal-organic frameworks based cathodes for enhancing electrochemical performances of batteries: A review," *ChemElectroChem*, vol. 6, no. 21, p. 5358-5374, 2019.

[46] Z. Liu, G. Pulletikurthi, and F. Endres, "A prussian blue/zinc secondary battery with a bio-ionic liquid–water mixture as electrolyte," *ACS Applied Materials & Interfaces*, vol. 8, no. 19, p. 12158-12164, 2016.

[47] Y. Xue, X. Shen, H. Zhou, J. Cao, J. Pu, Z. Ji, L. Kong, and A. Yuan, "Vanadium hexacyanoferrate nanoparticles connected by cross-linked carbon nanotubes conductive networks for aqueous zinc-ion batteries," *Chemical Engineering Journal*, vol. 448, p. 137657, 2022.

[48] F. A. Cotton, G. Wilkinson, C. A. Murillo, M. Bochmann, "Advanced inorganic chemistry" 6th edition, 1999: John Wiley & Sons. New York

[49] V. P. Prasadam, N. Bahlawane, F. Mattelaer, G. Rampelberg, C. Detavernier, L. Fang, Y. Jiang, K. Martens, I. P. Parkin, and I. Papakonstantinou, "Atomic layer deposition of vanadium oxides: Process and application review," *Materials Today Chemistry*, vol. 12, p. 396-423, 2019.

[50] K. Kosuge, T. Takada, and S. Kachi, "Phase diagram and magnetism of V_2O_3—V_2O_5 system," *Journal of the Physical Society of Japan*, vol. 18, no, 2, pp. 318-319, 1963.

[51] A. Heidemann, K. Kosuge, Y. Ueda, and S. Kachi, "Hyperfine interaction in V_3O_7," *Physica Status Solidi A*, vol. 39, no. 1, p. K37-K40, 1977.

[52] G. Nadkarni, and V. Shirodkar, "Experiment and theory for switching in Al/V_2O_5/Al devices," *Thin Solid Films*, vol. 105, no. 2, pp. 115-129, 1983.

[53] G. Nagaraju, and G.T. Chandrappa, "Solution phase synthesis of $Na_{0.28}V_2O_5$ nanobelts into nanorings and the electrochemical performance in Li battery," *Materials Research Bulletin*, vol. 47, no. 11, pp. 3216-3223, 2012.

[54] X. Zhang, D. Li, Q. Ruan, L. Liu, B. Wang, F. Xiong, C. Huang, and P. K. Chu, "Vanadium-based cathode materials for rechargeable magnesium batteries," *Materials Today Energy,* vol. 32, p. 101232, 2023.

55] L. Ma, L. Na, C. Long, B. Dong, F. Daliang, Z. Liu, Y. Zhao, X. Li, J. Fan, S. Chen, S. Zhang, and C. Zhi, "Achieving both high voltage and high capacity in aqueous zinc-ion battery for record high energy density. *Advanced Functional Materials*, vol. 29, no. 46, p. 1906142, 2019.

[56] M. S. Javed, H. Lei, Z. Wang, B-t. Liu, X. Cai, and W. Mai, "2D V_2O_5 nanosheets as a binder-free high-energy cathode for ultrafast aqueous and flexible Zn-ion batteries," *Nano Energy*, vol. 70, p. 104573, 2020.

[57] L. Shan, Y. Yang, W. Zhang, H. Chen, F. Guazhao, J. Zhou, and S. Liang, "Observation of combination displacement/intercalation reaction in aqueous zinc-ion battery," *Energy Storage Materials*, vol. 18, p. 10-14, 2019.

[58] U. Shankar, D. Govindarajan, C. Paul, J. Salethraj, F. J. Johanson, and M. D. Raja, "Enhanced the electrochemical properties of Ni doped V_2O_5 as a electrode material for supercapacitor applications," *Materials Today: Proceedings*, vol. 50, no. 4, pp. 2675-2678, 2022.

[59] D. Kundu, B. D. Adams, V. Duffort, S. H. Vajargah, and L. F. Nazar, "A high-capacity and long-life aqueous rechargeable zinc battery using a metal oxide intercalation cathode," *Nature Energy*, vol. 1, no. 10, p. 16119, 2016.

[60] Z. Wei, X. Wang, T. Zhu, P. Hu, L. Mai, and L. Zhou, "Mitigating the dissolution of V_2O_5 in aqueous $ZnSO_4$ electrolyte through Ti-doping for zinc storage," *Chinese Chemical Letters,* vol. 35, no. 1, p. 108421, 2024.

[61] F. Ming, H. Liang, Y. Lei, S. Kandambeth, M. Eddaoudi, and H. N. Alshareef, "Layered $Mg_xV_2O_5{\cdot}nH_2O$ as cathode material for high-performance aqueous zinc ion batteries," *ACS Energy Letters*, vol. 3, no. 10, pp. 2602-2609, 2018.

[62] Y. Yang, Y. Tang, S. Liang, Z. Wu, G. Fang, X. Cao, C. Wang, T. Lin, A. Pan, and J. Zhou, "Transition metal ion-preintercalated V_2O_5 as high-performance aqueous zinc-ion battery cathode with broad temperature adaptability," *Nano Energy*, vol. 61, pp. 617-625, 2019.

[63] F. Wu, Y. Wang, P. Ruan, X. Niu, D. Zheng, X. Xu, X. Gao, Y. Cai, W. Liu, W. Shi, and X. Cao, "Fe-doping enabled a stable vanadium oxide cathode with rapid Zn diffusion channel for aqueous zinc-ion batteries," *Materials Today Energy*, vol. 21, p. 100842, 2021.

[64] H. Cheng, X. Li, H. Hu, T. Yuan, S. Zhou, S. Dai, D. Zhang, and K. Pan, "Robust synthesis of a composite phase of copper vanadium oxide with enhanced performance for durable aqueous Zn-ion batteries," *Nanotechnology Reviews*, vol. 11, no. 1, pp. 1633-1642, 2022.

[65] S. Zheng, J. Chen, T. Wu, R. Li, X. Zhao, Y. Pang, and Z. Pan, "Rational design of Ni-doped V_2O_5@3D Ni core/shell composites for high-voltage and high-rate aqueous zinc-ion batteries," *Materials,* vol. 17, no. 1, p. 215, 2024.